RSC Advances

PAPER

View Article Online
View Journal | View Issue

Cite this: *RSC Adv.*, 2026, **16**, 16804

Experimental and theoretical investigations of porphyrin derivatives as corrosion inhibitors for carbon steel in acidic environments

Abd El-Aziz S. Fouda, *[a] Ahmed M. Elesawy,[b] Salah M. Rashwan,[b] Medhat M. Kamel,[b] Mohamed E. Eissa[c] and Hoyeda E. Ibrahim[b]

The corrosion inhibition effectiveness of two porphyrin molecules—5,10,15,20-tetrakis(4-phenoxyphenyl) porphyrin (PF-1) and 5,10,15,20-tetrakis(4-methoxyphenyl)porphyrin (PF-2)—on carbon steel (CS) immersed in 0.5 M H_2SO_4 solutions was investigated. The study utilized various techniques, as well as computational methods like Density Functional Theory (DFT) and Monte Carlo (MC) simulations, to determine the adsorption behavior and corrosion inhibition efficiency of PF-1 and PF-2 on the Fe(110) surface in an acidic environment. The surface morphology of CS was tested using different techniques. The inhibition efficiency (% η) of PF-1 and PF-2 was determined at a concentration of 21 $\times$ 10^{-6} M, 25 °C, reached 95.9%, 91.4%, respectively. This is depending on the substituent group present in the molecule. Increasing the temperature to 45 °C at the same 21 $\times$ 10^{-6} M concentration caused the efficiencies to decrease to 88.0% and 77.8%, respectively. Across all concentrations studied, the PF-1 molecule consistently exhibited a higher inhibitory efficacy than PF-2 due the presence of four Oph attached to the molecule, which increase both charge density on the molecule and the surface coverage of CS. The inhibitory action is attributed to the spontaneous physicochemical adsorption of the porphyrin molecules onto the CS surface, a process that conforms to the Langmuir adsorption isotherm. The PFs derivatives are considered mixed-kind inhibitors and proved to be the best inhibitors for CS dissolution in 0.5 M H_2SO_4. Additionally, thermodynamic activation parameters were calculated and analyzed.

Received 4th January 2026
Accepted 17th March 2026

DOI: 10.1039/d6ra00078a

rsc.li/rsc-advances

1 Introduction

Carbon steel (CS) is a fundamentally important industrial material in the modern world. It is an alloy composed primarily of iron with carbon and trace amounts of other metals.[1,2] "CS is used in many industries, including the oil and gas sector,[3] because of its exceptional qualities, which include outstanding mechanical strength, advantageous annealing and welding capabilities, and low cost.[4–6] However, the extremely acidic solutions used as solvents to dissolve subterranean rock formations can corrode the CS used in oil well exploration. These acidic solutions are critical for a variety of industrial activities, including the cleaning and descaling of steel, the removal of mud, the dissolution of rubble, and the creation of crucial channels for the flow of crude oil through rocks.[7] Recently, porphyrins have attracted a lot of attention as extremely potent corrosion inhibitors.[8,9] Their special properties—a macrocyclic structure, an extended π-electron system, and a significant affinity for binding metals—are what give them their effectiveness. The planar aromatic ring provides superior surface coverage and barrier protection, while the four pyrrolic nitrogen atoms enable strong chemisorption straight onto metallic surfaces. Particularly in harsh acidic conditions, these structural characteristics allow porphyrins and their metal complexes to efficiently prevent both anodic dissolution (metal oxidation) and cathodic hydrogen evolution (reduction process). Additionally, porphyrins are a prospective class of environmentally acceptable, high-performance corrosion inhibitors for a variety of metal systems, including steel, copper, and aluminum, due to their tunable substituents, superior thermal and chemical stability, and comparatively low environmental toxicity. Most synthesized porphyrins have potential use in medical and pharmaceutical chemistry.[10–12] It was successful to use organic composites and their byproducts as inhibitors for various steel kinds. In acidic environments, several organic molecules containing heteroatoms of nitrogen, oxygen, and sulfur have been proposed as steel inhibitors.[13] Because these composites function as inhibitors by surface adsorption, the shape of the metal surface and the electrochemical potential at the interface are just two of the many

[a]*Chemistry Department, Faculty of Science, Mansoura University, Mansoura-35516, Egypt. E-mail: asfouda@mans.edu.eg*

[b]*Department of Chemistry, Faculty of Science, Suez Canal University., Egypt*

[c]*Chemistry Department, College of Science, Imam Mohammad Ibn Saud Islamic University (IMSIU), Riyadh 11623, Saudi Arabia*

variables that affect an inhibitor's efficacy. The majority of organic inhibitors are costly, hazardous, and have negative environmental implications, which limits their usage in preventing metal dissolution. Therefore, it is crucial to improve inexpensive and ecologically friendly corrosion protection.[14,15] The impact of organic compounds on metal corrosion in corrosive conditions has been covered by numerous writers in the review.[16–18] These materials can stick to the steel's surface, blocking the active sites and reducing the rate of corrosion. The present study investigated the effect of organic inhibitors on the dissolution of CS in 0.5 M H_2SO_4. Its core contains the molecular structure of a potential corrosion inhibitor. It is a tetradentate chelating agent that may clearly interact with surfaces through a range of chemical and/or physical mechanisms and has a high bonding capacity.[19] Metal-porphyrin complexes are helpful model molecules for metalloenzymes and electron transport in biological systems. Porphyrins are also frequently utilized as stationary phases in high-pressure liquid chromatography (HPLC), biosensors, catalysis, photovoltaic cells, membrane components for ion-selective electrodes, and ligands for spectrophotometric cation determination.[20–22] There have also been reports of their use as carbon steel corrosion inhibitors in aqueous mineral acid.[23,24] Porphyrin molecules can reorganize the electron distribution of their conjugated aromatic rings to form ordered molecular layers on electrode surfaces, according to multiple findings on the corrosion inhibition characteristics of various porphyrin molecules. These molecular layers act as a barrier that stops electroactive substances from diffusing toward the metal surface. Numerous factors, including electron density at donor centers, steric hindrance, and peripheral functional groups, influence the adsorption of porphyrin molecules and their corrosion inhibition characteristics.[25] Jaafar *et al.*[26] synthesized some porphyrins derivatives, these are termed as 4,4′,4″,4‴-(porphyrin-5,10,15,20-tetrayl)tetrakis(*N*-(6-aminoacridin-3-yl)benzamide) (**3a**), 4,4′,4″,4‴-(porphyrin-5,10,15,20-tetrayl)tetrakis(*N*-(5-methoxybenzo[*d*]thiazol-2-yl)benzamide) (**3b**), 4,4′-(10,20-bis(3-hydroxyphenyl)porphyrin-5,15-diyl)bis(*N*-(6-aminoacridin-3yl) benzamide) (**5a**), and 4,4′-(10,20-bis(3-hydroxyphenyl) porphyrin-5,15-diyl)bis(*N*-(benzo[*d*]thiazol-2-yl)benzamide) (**5b**) and employed them as CS corrosion inhibitors in a 0.1 M HCl solution. The maximal inhibition efficiency (% η) for derivative

Table 1 % Inhibition efficacy for porphyrin derivatives as corrosion inhibitors in various medium

Extract	Sample	Medium	Inhibition efficacy (% η)	Ref.
5,10,15,20-Tetra (thiophen-2-yl)porphyrin (P1) and 5,10,15,20-tetrakis (5-bromothiophen-2-yl) porphyrin (P2)	Stainless steel 304 (SS304)	2 M HCl	92.5%, 88.5% at 21 $\times$ 10^{-6} M for P1 & P2, respectively	30
Tetraphenyldithiaoctaase cyclotetradecane hexane	Steel	3.0 M HCl	90% at = 500 mg L^{-1}	31
5,10,15,20-Tetraphenylporphyrin (TPP)	Iron	0.5 M H_2SO_4	81.3% at 17 hours	32
5,10,15,20-Tetrakis (4-pyridyl)-21*H*,23*H*-porphin (TPyP)	Mild steel	5% H_2SO_4	Reduces the corrosion rate of steel by more than 50%	33
5,10,15,20-20-Tetra (4-methylphenyl)-21*H*,23*H* porphyrin	Mild steel	0.1 M H_2SO_4	80%	34
5,10,15,20-Tetrakis (4-hydroxyphenyl)21*H*,23*H*-porphyrin (HPTB), 5,10,15,20-tetra(4-pyridyl)-21*H*,23*H*-porphyrin (T4PP), 4,4′,4‴,4⁗-(porphyrin-5,10,15,20-tetrayl)tetrakis (benzoic acid) (THP) and 5,10,15,20-tetraphenyl-21*H*,23*H*-porphyrin (TPP)	N80 steel in	3.5% NaCl	85% to 91%	35
5,10,15,20-Tetrakis(pentafluorophenyl)-21*H*,23*H* palladium(II) porphyrin (PF-1) and 4,4′,4‴,4⁗-(porphyrin-5,10,15,20-tetrayl)tetrakis (benzoic acid) (PF-2)	J55 steel	CO_2	PF-2 > PF-1, by about 93%, at a concentration of 0.4 mM	36
5,10,15,20-Tetrakis(4-phenoxyphenyl)porphyrin (PF-1), 5,10,15,20-tetrakis (4-methoxyphenyl)porphyrin	Carbon steel	0.5 M H_2SO_4	95.9%, 91.4% at 21 $\times$ 10^{-6} M, respectively	Our results

Compound	PF-1	PF-2
Structure	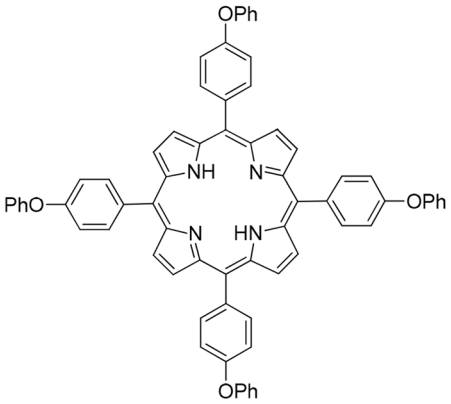	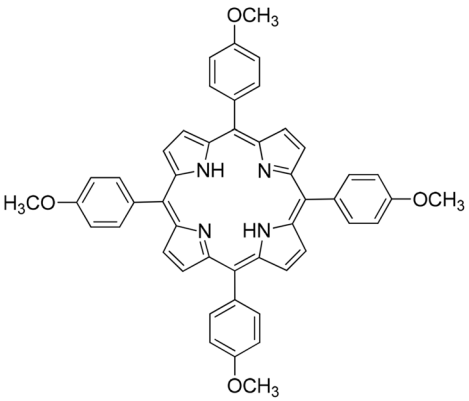
	5,10,15,20-tetrakis(4-phenoxyphenyl) porphyrin	5,10,15,20-tetrakis(4-methoxyphenyl) porphyrin
Mol. Formula	$C_{68}H_{46}N_4O_4$	$C_{48}H_{38}N_4O_4$
Mol. Wt.	MW = **983.14** g/mol	MW = **734.84** g/mol

Fig. 1 Chemical structure of the organic inhibitors (PF-1 & PF-2).

3a was found to be approximately 74%. The % η of derivative **3b** was approximately 68.11%, whereas the % η of derivatives **5a** and **5b** were approximately 18.98% and 45.16%, respectively.

In the case of the derivative **3a**, a maximum inhibition efficiency (IE%) was recorded and it was around 74%". The derivative **3b** showed an IE% of around 68.11%, while the % η of **5a** and **5b** were around 18.98% and 45.16%, respectively.[27]

Two novel organic corrosion inhibitors: 1-benzyl-5-methyl-*N*′-(1-(thiophen-2-yl)ethylidene)-1*H*-pyrazole-3-carbohydrazide (Pyr1) and 1-benzyl-5-methyl-*N*′-(1-(pyridin-2-yl)ethylidene)-1*H*-pyrazole-3-carbohydrazide (Pyr2) were synthesized and characterized and utilized as corrosion inhibitors for carbon steel in 1 M HCl solution.[28] Their inhibition performance (% η) was evaluated through electrochemical and weight loss measurements, revealing that % η increased with both rising temperature and concentrations of Pyr1 and Pyr2. At 10^{-3} M and 298 K, PDP measurements showed 90.48% and 93.77% inhibition efficiencies for Pyr1 and Pyr2, respectively, three novel water-soluble amino acids benzimidazole derivatives (1-amino-1-(1*H*-bezo[*d*] imidazole-2-yl-2-ol, B1), 1-(1*H*-bezo[*d*]imidazole-2-yl)-3-methylbutan-1-amine, B2, and1-(1*H*-benzo[*d*]imidazole-2-yl)-3-(methylthio)propan-1-amine, B3) were synthesized and used for the protection of carbon steel (X56) against corrosion in 1 M HCl solution.[29] Table 1 shows the use of some organic compounds as inhibitors for metals and alloys in various media. The results showed a maximum protective efficiency range between 95% and 98% indicating high corrosion inhibition. The porphyrin derivatives used in this work are readily available, non-toxic, have greater molecular weights, highly soluble in water, and comprise a significant number of donating atoms (N and O).

In the present study, two porphyrin compounds namely 5,10,15,20-tetrakis(4-phenoxyphenyl)porphyrin (PF-1) & 5,10,15,20-tetrakis(4-methoxyphenyl)porphyrin (PF-2) were investigated for their inhibition potentials on the corrosion of CS in 0.5 M H_2SO_4 solution. Experimental techniques such as electrochemical impedance spectroscopy (EIS), potentiodynamic polarization (PDP), and surface examination have been used to study the corrosion inhibition mechanism and determine the inhibition efficiencies of the studied porphyrins. The structures of the four porphyrins used as corrosion inhibitors in the present study are shown in Fig. 1.

2 Experiment

2.1 Carbon steel samples

The material employed in this study was carbon steel with the following chemical composition (wt%): 0.21% C, 1.22% Mn, 0.24% Si, 0.045% P, 0.036% S, with the remainder being Fe. Carbon steel (CS) specimens measuring 2 × 2 × 0.2 cm were prepared in triplicate and mechanically polished. The samples were successively abraded using emery papers of grades 600, 800, 1000, and 1200, thoroughly rinsed several times with bidistilled water, degreased with acetone to remove any oil residues, dried using filter paper according to a strict surface preparation protocol, and finally weighed to determine their initial mass.

2.2 Chemicals

2.2.1 Porphyrin derivatives (PF-1 and PF-2) preparation. Porphyrin derivatives (PF-1 and PF-2) were prepared according to the previously reported work.[37,38] Meso-porphyrin derivatives PF-1

and PF-2 were obtained by condensing aldehyde derivatives with pyrrole in the presence of *p*-ToSH. Acid-catalyzed addition of pyrrole to the substituted benzaldehyde carbonyl group, followed by acid-catalyzed dehydration, is the mechanism for porphyrin synthesis. This procedure is repeated to add an additional benzaldehyde moiety. The reduced form of porphyrin (porphyrinogen) is obtained because of ring closure, and the porphyrin building blocks are then produced through oxidation. The DMF molecule would serve as an excellent leaving group each time more pyrrole is added. The DMF-capped reactive species combine with additional pyrrole to continue to produce the appropriate porphyrinogen as in Scheme 1.

2.2.2 Solutions. An appropriate concentration of 0.5 M H_2SO_4 was prepared by the dilution of AR grade (H_2SO_4, BDF 98%) with bidistilled water. To acquire different inhibitor concentrations, a (1×10^{-3} M) stock solution of porphyrin derivatives were diluted with bidistilled water (1–21 $\times$ 10^{-6} M).

2.3 Chemical tests (mass reduction, MR)

The weight loss procedure was conducted in accordance with the ASTM G31–72 standard method.[39] To do this, test coins made of carbon steel (CS) were submerged in 100 mL of 0.5 M H_2SO_4 solution and subjected to varying concentrations of the porphyrin (PF-1, PF-2) composites under investigation at a temperature range from 298 to 318 K in a temperature-controlled oven.[40] After the CS samples were removed from the test solutions, they were promptly cleaned with bidistilled water and left to air dry, and their final weights were noted after the period of 180 minutes. Over a predetermined, the average (MR) for the tested samples was computed in mg cm^{-2}. By weighing the steel coupons both before and after immersion, the mass changes were measured. The corrosion rate (measured in mg cm^{-2} min^{-1}) and the percentage of corrosion prevention efficiency (%) were then computed using the resultant MR difference data. The MR (ΔW) of CS pieces at different time intervals, both in the absence and presence, precisely (1–21 $\times$ 10^{-6} M) of the examined composites, was obtained from the corrosion experiments". The following relation, usually referred to as eqn (1), is used to compute the value for ΔW:[41]

$$\Delta W = \frac{W_1 - W_2}{a} \quad (1)$$

where W_1 and W_2 are the specimens' mass prior to and following the reaction, respectively, and the surface area in centimeters. IE % was calculated using eqn (2):

$$\%\ \eta = \frac{\Delta W - \Delta W_i}{\Delta W} \times 100 \quad (2)$$

where ΔW and ΔW_i represent the mass decreased per unit area in the absence and presence of the examined composite, respectively. The experiments were conducted in triplicate to ensure the reliability of our results.

2.4 Electrochemical tests

2.4.1 Potentiodynamic polarization (PDP) technique. To better comprehend electrochemical impedance spectroscopy (EIS) and potentiodynamic polarization methods were carried out. The main objective was to fully assess how well the porphyrin (PF-1, PF-2) composites inhibited corrosion. The electrochemical measurements were carried out using a conventional three-electrode system, comprising a CS electrode as the working electrode, platinum as the counter electrode, and a saturated calomel electrode (SCE) as the reference electrode.[42] A Gamry Potentiostat/Galvanostat was used to conduct these tests. A CS working electrode that displayed a 1 $\times$ 1 cm^2 exposed area on one side served as the setup's central component. Prior to the measurements, the working electrode was immersed in the test solution for 30 minutes to achieve a stable open circuit potential (OCP). For the polarization studies, the potential was scanned within a range of $\pm$250 mV at a scan rate of 0.2 mV s^{-1}. The following formula is used to evaluate the corrosion inhibition effect, which is developed from the PDP experiment values in 0.5 M H_2SO_4:[43]

$$\%\ \eta = \left(1 - \left(i_{corr}/i^{\circ}_{corr}\right)\right) \quad (3)$$

In this case, i_{corr} and i°_{corr} represent the presence and absence of corrosion porphyrin, respectively.

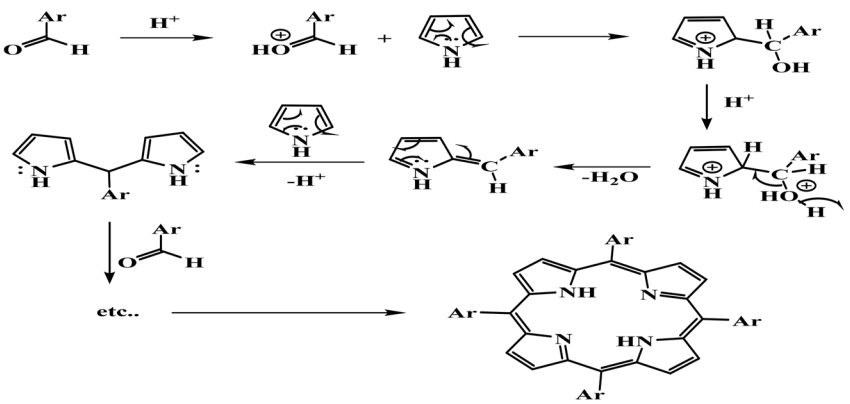

PF-2, Ar= C_6H_4-OPh-*p*; PF-1, Ar= C_6H_4-OCH_3-*p*

Scheme 1 Preparation of porphyrin derivatives (PF-1 and PF-2).

2.4.2 Electrochemical impedance spectroscopy (EIS) technique. The Open Circuit Potential (OCP) was used for the EIS investigation. The frequencies were swept from 10^5 Hz to 0.01 Hz using an alternating current (AC) pulse with an amplitude of 10 mV. This method was used to calculate the double-layer capacitance (C_{dl}) and evaluate the compound's inhibitory efficacy. The following formula is used to assess the inhibition efficiency based on the EIS experimental values:[44]

$$\% \eta = \left(R_{ct}^{*} - R_{ct}\right)/R_{ct}^{*} \times 100 \quad (4)$$

$$C_{dl} = 1/2\pi f_{max} R_{ct} \quad (5)$$

where R_{ct}^{*} and R_{ct} represent the charge transfer resistance of the metal with and without the corrosion inhibitor chemicals, respectively, and f_{max} represents the maximum impedance frequency.

Echem Analyst 5.5 software was used to analyze electrochemical data. The working electrode was submerged in the solution until a steady state was reached (30 minutes) before to starting the test. All electrochemical experiments conducted in this study were performed in triplicate to ensure reproducibility of the results.

2.5 Surface morphological studies (SEM-EDX and AFM spectroscopy)

After metallic coupons were immersed in a 0.5 M H_2SO_4 solution, their external morphology (surface structure) was examined analytically. "In this study, two conditions were compared: the corrosive solution with and without 21 × 10^{-6} M of the inhibitors present. The samples were initially submerged in the inhibitor at 298 K for a whole day. We used two main analytical methods for our study's surface investigation. First, an Energy-Dispersive X-ray (EDX) analyzer connected to a scanning electron microscope (SEM, model SNE-3200M) was used to evaluate the elemental analysis of the carbon steel specimen. A separate SEM (JSM-6510LV, Japan) operating at 30 kV was used to evaluate the surface morphology, and an EDX device operating at 20 kV was used to determine its elements composition.[31] The average surface texture values of the steel surfaces were examined using Atomic Force Microscopy (AFM)". A Nanosurf device (module: Easy Scan 2, made in Switzerland) was used for this investigation. Surfaces treated with PF-1 and PF-2 were compared to those without the inhibitors in the analysis.

2.6 Computational chemical approaches

Materials Studio version 7.0's density functional theory (DFT) was used to examine the connection between NOL's molecular structure and reactivity. Quantum chemical studies using DFT were used to study the organic inhibitors. "The initial portion of our study focused on the geometrical optimization of organic corrosion inhibitors using the Gaussian 16 program, the B3LYP functional, and the 6-31G/(d, P) basis set. These optimizations allowed for a comprehensive understanding of the molecular structures in both gaseous and aqueous environments. To thoroughly assess the electronic properties of the inhibitors, we calculated important parameters as E_{HOMO}, E_{LUMO}, hardness (η), energy gaps (ΔE), softness (σ), and dipole moment (μ). After then, these elements were investigated and analyzed. The corrosion inhibitors' reactivity, which indicated their potential for chemical interactions, was assessed using Fukui indices". Important variables like hardness (η) and softness (σ), which are strongly related to E_{HOMO} and E_{LUMO} as demonstrated by the following equation, have a significant impact on the effectiveness of organic inhibitors:

$$\eta = \tfrac{1}{2}(E_{HOMO} - E_{LUMO}) \quad (6)$$

$$\sigma = 1/\eta \quad (7)$$

In order to better understand the areas of electrophilic and nucleophilic interactions of the corrosion inhibitor molecule, we also performed Fukui function calculations using the following equation.

$$f_k^{+} = q_k\,(N+1) - q_k\,(N) \text{ nucleophilic} \quad (8)$$

$$f_k^{+} = q_k\,(N) - q_k\,(N-1) \text{ electrophilic} \quad (9)$$

3 Result and discussion

3.1 Mass reduction (MR) test

Fig. 2 displays the calculated mass reduction for CS at 25 ± 1 °C with and without adjusted concentrations of PF-1 and PF-2 of the investigated compounds in the concentration range of 1 × 10^{-6} M to 21 × 10^{-6} M. The data for inhibitory efficiency (IE), corrosion rate (CR), and surface coverage were calculated and compiled in Table 2 based on the mass reduction investigation. Fig. 2 shows how weight loss changed over time in PF-1 and PF-2 inhibited and unregulated solutions. The effectiveness of inhibition increases with the inhibitor's concentration. Higher inhibitor concentrations enhance the effectiveness of adsorption onto the metal surface, creating a barrier that keeps corrosive substances from meeting the metal. Indeed, the inhibitory impact of PF-1 and PF-2 was concentration-dependent. Thus, the maximum inhibition efficiency was determined to be 95.4% and 91.4%, respectively, using 21 × 10^{-6} M of PF-1 and PF-2. The results demonstrated that PF-1 suppresses the metal's rate of corrosion more effectively than PF-2. This might be the result of PF-1's higher molecular size and two benzene rings compared to PF-2.

3.2 Effect of temperature on the corrosion process

3.2.1 Kinetic-thermodynamic corrosion parameters. The adsorption of organic molecules on the iron's surface protects the exposed CS coupons' reactive areas from corrosion in a 1 M hydrochloric acid solution, reducing the rate of corrosion (Table 3) and boosting the effectiveness of modified corrosion inhibitor molecules. "However, it was demonstrated that the temperature increase increased the CR in both inhibited and uninhibited solutions. This suggests that the steel is more susceptible to deterioration when the temperature agitation of the corrosive fluid increases. In a 1 M hydrochloric acid

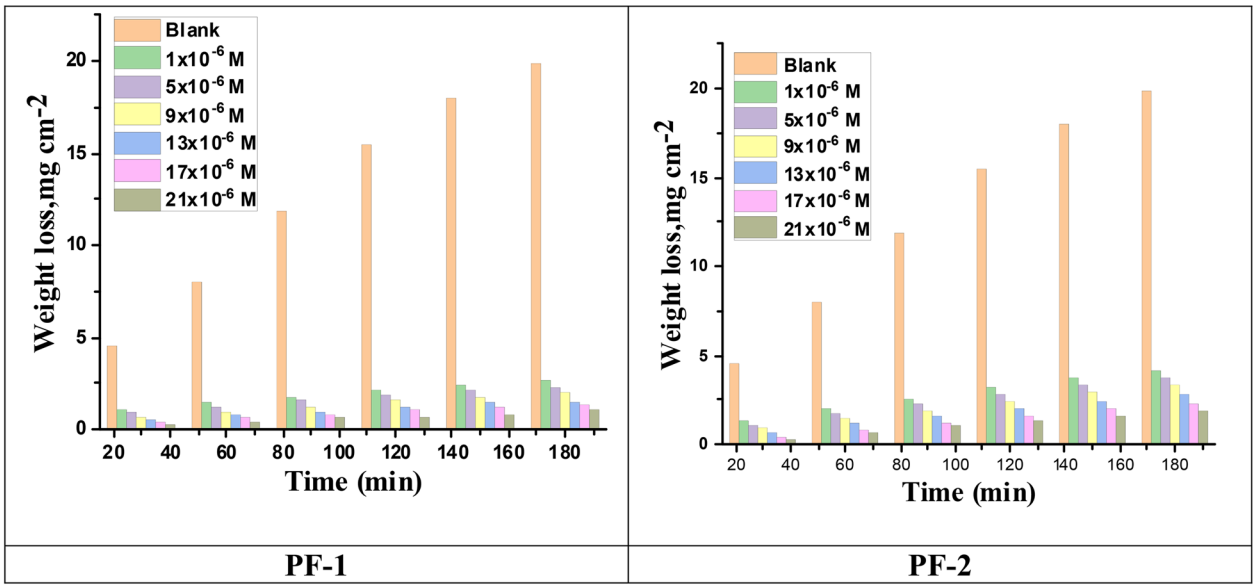

Fig. 2 Time-MR bends of CS in H_2SO_4 attendance and lack various concentrations of compounds (PF-1 & PF-2) at 25 °C.

solution, the exposed CS coupons' reactive portions are shielded from corrosion by the adsorption of organic molecules on the iron's surface, which lowers the rate of corrosion (Table 3) and increases the efficacy of modified corrosion inhibitor molecules. However, it was shown that in both inhibited and uninhibited solutions, the CR increased as the temperature climbed". This indicates that the steel is more prone to deterioration when the corrosive medium's temperature rises, which is a sign of the physisorption adsorption process.[45]

The influence of CR on temperature expressed by Arrhenius-type equation:[46]

$$R_{corr} = A \exp\left(\frac{-E_a^*}{RT}\right) \quad (10)$$

Depending on the kind of metal and electrolyte, "A" is the Arrhenius pre-exponential constant and "R_{corr}" is the CR. Fig. 3 graphically depicted the logarithm of the corrosion rate (log R_{corr}) with the reciprocal of absolute temperature ($1/T$) in the absence and presence of porphyrin PF-1 & PF-2. Fig. 4 graphically depicts plots of the logarithm of the corrosion rate by temperature ($\log R_{corr}/T$) with the reciprocal of absolute temperature ($1/T$) in the presence and absence of porphyrin PF-1 & PF-2. Table 4 summarizes the values of activation energy (E_a^*), enthalpy changes of activation (ΔH^*), and entropy change of activation (ΔS^*). It suggests that the whole process is controlled by surface reaction since (E_a^*) of the corrosion process is over (20 kJ mol^{-1}). The (ΔH^*) and (ΔS^*) for corrosion of CS in 0.5 M H_2SO_4 in the absence and presence of PF-1 & PF-2 are calculated from the transition state theory using the following equation".[47]

$$R_{corr} = \frac{RT}{Nh}\exp\left(\frac{\Delta S^*}{R}\right)\exp\left(\frac{-\Delta H^*}{RT}\right) \quad (11)$$

where R is the gas constant, N is Avogadro's number, and h is Planck's constant. Table 4 lists the calculated values of ΔH^* and ΔS^*. (E_a^*) values rose, which in turn reduced the CS's rate of corrosion. The endothermic nature of the CS dissolving process

Table 2 IE%, CR, and of PF-1 and PF-2 compounds at different concentrations following a 120 minutes CS test in a 0.5 M H_2SO_4 solution at 25 °C

Compound	Conc., $\times 10^{-6}$ M	CR $\times$ 10^{-2} M mg (cm^{-2} min^{-1})	θ	% η
	Blank	0.1287 ± 0.002	—	—
PF-1	1	0.0179 ± 0.005	0.861	86.1
	5	0.0153 ± 0.003	0.881	88.1
	9	0.0130 ± 0.004	0.899	89.9
	13	0.0104 ± 0.001	0.919	91.9
	17	0.0085 ± 0.004	0.934	93.4
	21	0.0059 ± 0.004	0.954	95.4
PF-2	1	0.0264 ± 0.002	0.795	79.5
	5	0.0232 ± 0.005	0.820	82.0
	9	0.0200 ± 0.003	0.845	84.5
	13	0.0162 ± 0.001	0.874	87.4
	17	0.0127 ± 0.003	0.901	90.1
	21	0.0111 ± 0.002	0.914	91.4

Table 3 η % and CR of PF-1, PF-2 compounds at various concentrations, and temperatures after dipping CS for 120 min in 0.5 M H_2SO_4 solution

		30 °C		35 °C		40 °C		45 °C	
Inh.	Conc, $\times 10^6$ M	CR	% η	CR	% η	CR	% η	CR	% η
	Blank	0.1703 ± 0.002	—	0.2263 ± 0.003	—	0.2968 ± 0.003	—	0.3145 ± 0.005	—
PF-1	1	0.0262 ± 0.002	84.6	0.0425 ± 0.004	81.2	0.0588 ± 0.002	80.2	0.0670 ± 0.001	78.7
	5	0.0240 ± 0.001	85.9	0.0367 ± 0.003	83.8	0.0534 ± 0.001	82.0	0.0591 ± 0.003	81.2
	9	0.0175 ± 0.002	89.7	0.0308 ± 0.002	86.4	0.0490 ± 0.003	83.5	0.0569 ± 0.002	81.9
	13	0.0160 ± 0.003	90.6	0.0247 ± 0.005	89.1	0.0442 ± 0.004	85.1	0.0516 ± 0.003	83.6
	17	0.0141 ± 0.004	91.7	0.0210 ± 0.002	90.7	0.0344 ± 0.005	88.4	0.0456 ± 0.004	85.5
	21	0.0119 ± 0.004	93.0	0.0167 ± 0.004	92.6	0.0291 ± 0.003	90.2	0.0377 ± 0.004	88.0
PF-2	1	0.0412 ± 0.001	75.8	0.0638 ± 0.003	71.8	0.1000 ± 0.004	66.3	0.1173 ± 0.003	62.7
	5	0.0351 ± 0.003	79.4	0.0575 ± 0.001	74.6	0.0890 ± 0.005	70.0	0.1082 ± 0.001	65.6
	9	0.0303 ± 0.005	82.2	0.0520 ± 0.001	77.0	0.0807 ± 0.002	72.8	0.0991 ± 0.003	68.5
	13	0.0264 ± 0.002	84.5	0.0455 ± 0.002	79.9	0.0712 ± 0.003	76.0	0.0878 ± 0.002	72.1
	17	0.0209 ± 0.001	87.7	0.0382 ± 0.002	83.1	0.0629 ± 0.004	78.8	0.0761 ± 0.004	75.8
	21	0.0179 ± 0.001	87.7	0.0296 ± 0.002	85.1	0.0522 ± 0.005	80.6	0.0642 ± 0.001	77.8

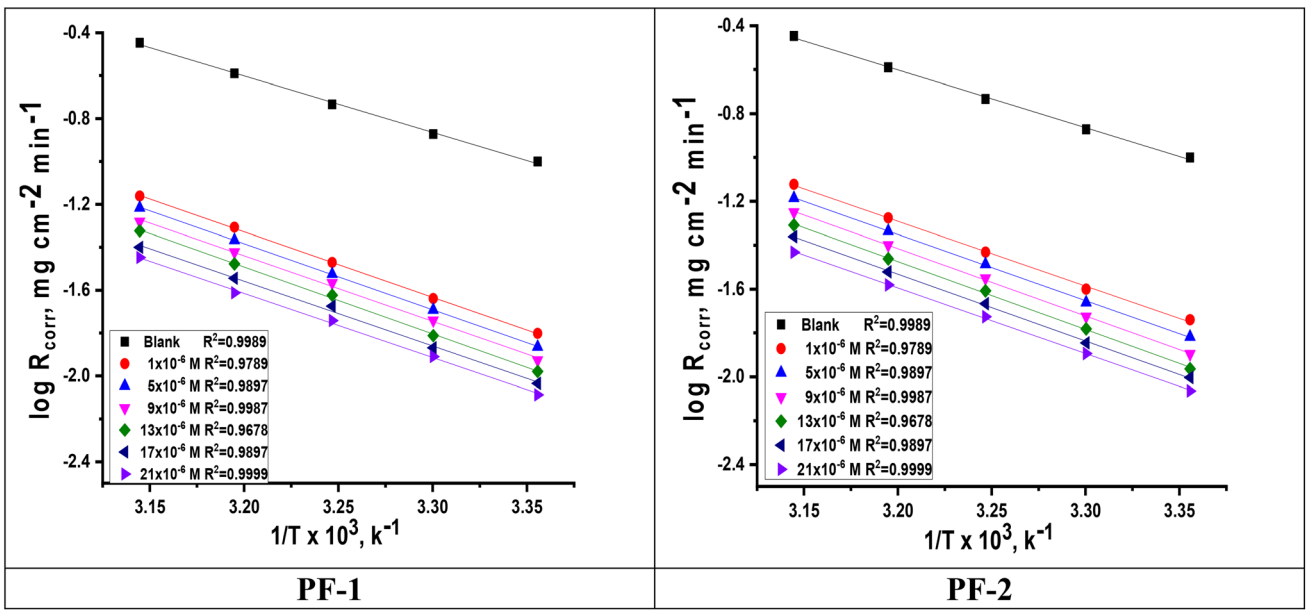

Fig. 3 Log CR *vs.* 1/*T* of porphyrin (PF-1 & PF-2) and free sample at temperature range 25–45 °C.

is indicated by the positive values of (ΔH^*). Because of the decrease in disorder that occurs as the transition from reactants to the activated complex progresses, the values (ΔS^*) are substantial and negative".[48]

3.2.2 Adsorption isotherm behavior. One helpful technique for understanding the corrosion process is adsorption isotherm analysis. Additionally, it allows for a deeper understanding of the connection between CS and inhibitors. The best-fit adsorption isotherm was identified using surface coverage data from MR measurements. The experimental results were appropriately analyzed using several adsorption isotherm models, such as Freundlich, Temkin, and Langmuir. The results were most accurate when analyzed using the Langmuir isotherm. The fractional surface coverage (C/θ) is shown against the molecule concentrations (C) at temperatures ranging from 25 to 45 °C in the graphs' straight-line plots, as seen in Fig. 5". The following eqn (12) was used to determine the values of the corrosion inhibitor's adsorption constant (K_{ads}).

$$\frac{C_{inh}}{\theta} = \frac{1}{K_{ads}} + C_{inh} \quad (12)$$

where C is the inhibitor concentration, θ is the degree of surface coverage of the inhibitor molecule, and K_{ads} is the adsorption equilibrium constant. "Fig. 5 shows the Langmuir adsorption isotherm plots. Comparison of the adsorption data indicated that the Langmuir isotherm most accurately described the experimental results, as evidenced by the highest correlation coefficient (R^2) values and slopes for PF-1 and PF-2 at different temperatures that were close to unity. These findings suggest that the adsorption of the inhibitors on the CS surface follows the Langmuir model, which assumes monolayer adsorption

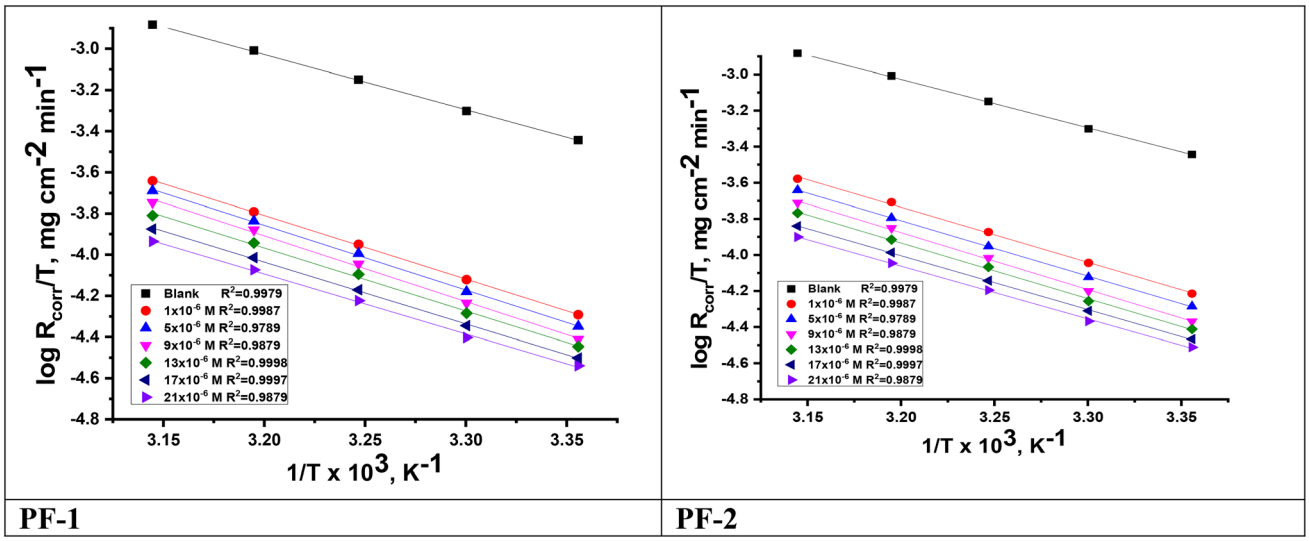

Fig. 4 Log(CR/*T*) *vs.* 1/*T* of porphyrin (PF-1 & PF-2) and free sample at temperature range 25–45 °C.

Table 4 Activation parameters of the liquefaction of CS in 0.5 M H_2SO_4 with and without of porphyrin PF-1 & PF-2 at 25–45 °C

Inhibitor	Conc., $\times 10^6$ M	Activation parameters		
		E_a^* kJ mol^{-1}	ΔH^* kJ mol^{-1}	$-\Delta S^*$ J mol^{-1} K^{-1}
Blank	—	50.7	48.2	125.2
PF-1	1	70.2	67.7	75.4
	5	71.6	69.1	71.6
	9	72.5	70.0	68.8
	13	73.3	70.8	67.1
	17	74.1	71.6	65.8
	21	74.8	72.3	65.2
PF-2	1	68.1	65.6	73.2
	5	70.3	67.8	67.6
	9	70.9	68.4	66.6
	13	71.6	69.1	65.4
	17	71.9	69.4	64.6
	21	72.8	70.3	63.3

without interactions among the adsorbed species. Table 5 demonstrates that the corrosion inhibitors from the steel exterior desorb when the temperature rises because the K_{ads} value decreases". The K_{ads} value, which is connected to the Gibbs free energy change (ΔG°_{ads}), was obtained from the intercept ($1/K_{ads}$):

$$K_{ads} = (1/55.5) \times \exp\left(-\Delta G^\circ_{ads}/RT\right) \quad (13)$$

whereas $-\Delta G^\circ_{ads}$ the standard free adsorbent, a solution containing 55.5 molar water. "Fig. 5 shows the plot of C/θ *vs.* C for the PF-1 and PF-2 in the tested solutions. Table 5's slope, R^2, K_{ads}, and ΔG°_{ads} demonstrate a significant interaction between the iron exterior and the inhibitor compounds. The durability of the adsorbed layer and spontaneous adsorption on the CS surface caused the negative sign of ΔG°_{ads}.[49] Furthermore, the stability of K_{ads} with increasing temperature confirms the strong contact between the corrosion inhibitors and the steel exterior. Gibb's free energy values of 20 kJ mol^{-1} or below generally indicate physisorption adsorption regulated by electrostatic forces. On the other hand, values greater than 40 kJ mol^{-1} suggest chemisorption adsorption; results between 20 and 40 kJ mol^{-1} imply chemisorption adsorption through bonding between metal ions and inhibitor atoms. The conventional free energy of adsorption value is predicted to be between 23.2 and 21.1 kJ mol^{-1}, as shown in Table 5. This value is within the range of competitive interactions between chemical and physical adsorption processes. In acidic solutions, cationic species may adsorb on mild steel cathodic sites, delaying the formation of hydrogen. This material lessens the anodic dissolution of carbon steel by sticking to anodic sites with nitrogen, chlorine, and phenyl groups.[50] K_{ads} readings are used to organize compounds: Strong metal surface contact and corrosion inhibition were indicated by PF-1 > PF-2, which had the highest negative free energy of adsorption. The heat of adsorption (ΔH°_{ads}) can be calculated using the Van't Hoff equation as follows.[51] Plotting log K_{ads} with $1/T$ for CS in 0.5 M H_2SO_4 with porphyrin (PF-1 & PF-2) is shown in Fig. 6. Adsorption is exothermic because the heat of adsorption is negative. Adsorption can be either chemical or physical in an exothermic process, whereas it can only be chemical in an endothermic process". The values ΔH°_{ads} are less than 100 kJ mol^{-1}, representative that the physisorption".[47]

$$\text{Log } K_{ads} = \Delta H^\circ_{ads}/2.303RT + \text{constant} \quad (14)$$

Finally, using the next equation, ($-\Delta S^\circ_{ads}$) was determined:

$$\Delta S^\circ_{ads} = \left(\Delta H^\circ_{ads} - \Delta G^\circ_{ads}\right)/T. \quad (15)$$

3.3 Electrochemical measurements

3.3.1 PDP measurements. PDP bending of CS is shown in Fig. 7 in "0.5 M H_2SO_4 in the attendance and lack of altered concentrations of the investigated compounds (PF-1 & PF-2).

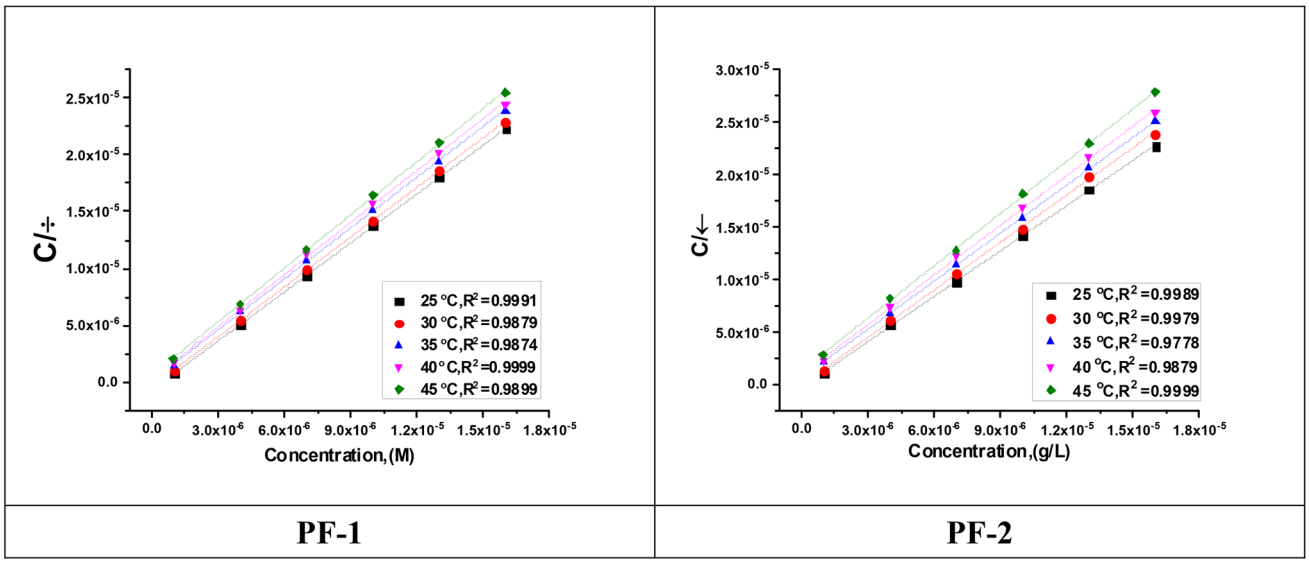

Fig. 5 Langmuir bends of porphyrin PF-1 & PF-2 on CS surface in 0.5 M H_2SO_4 at various temperatures.

Table 5 Thermodynamic parameters obtain from Langmuir

Inhibitor	Temp., K	R^2	K_{ads} M^{-1}	$-\Delta G^{\circ}_{ads}$ kJ mol^{-1}	$-\Delta H^{\circ}_{ads}$ kJ mol^{-1}	$-\Delta S^{\circ}_{ads}$ J mol^{-1} K^{-1}
PF-1	298	0.9998	207	23.2	32.0	77.6
	303	0.9987	165	22.9		75.74
	308	0.9999	130	22.7		73.7
	313	0.9989	108	22.6		72.2
	318	0.9879	91	22.5		70.8
PF-2	298	0.9999	187	22.9	38.0	76.7
	303	0.9999	145	22.6		74.6
	308	0.9987	110	22.3		72.3
	313	0.9998	88	22.1		70.5
	318	0.9987	71	21.8		68.7

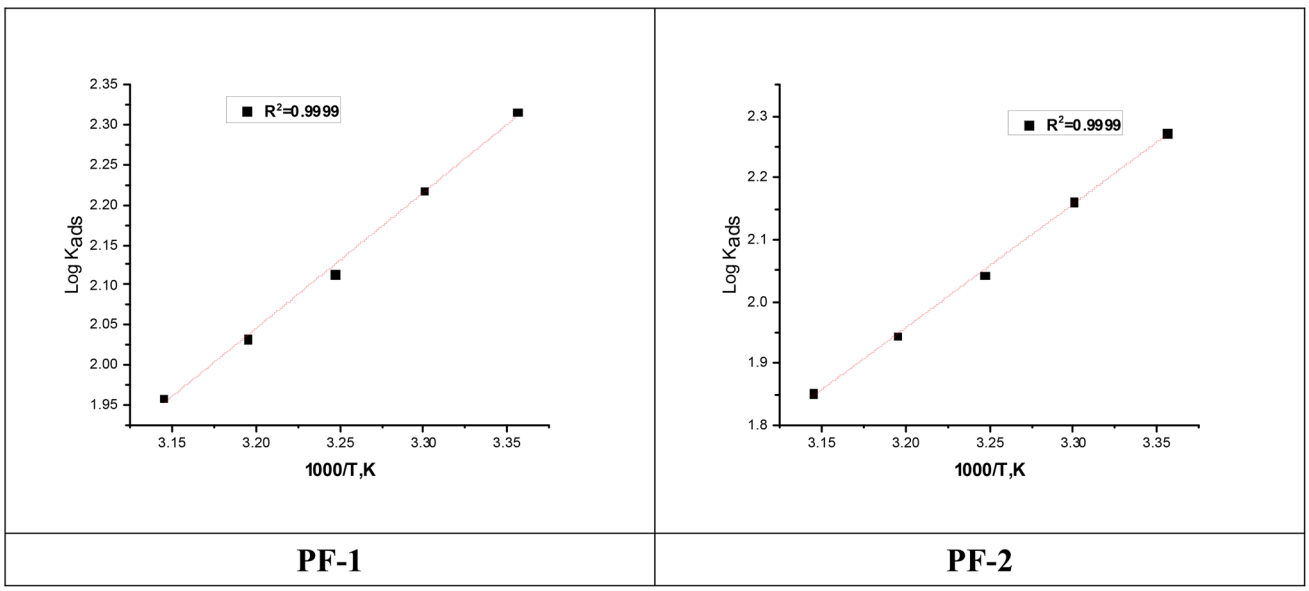

Fig. 6 Log K_{ads} *vs.* 1000/*T* plots obtained from Langmuir isotherm.

The electrochemical parameters determined *via* Tafel extrapolation at E_{corr}, such as i_{corr}, β_a, and β_c, are listed in Table 6. It has been shown that the current density falls when porphyrin PF-1 and PF-2 concentrations rise. The polarization curves and eqn (3) were used to calculate IE%. The inhibition of these processes becomes increasingly apparent as the inhibitor concentration increases, increasing the inhibition efficiency. When the inhibitors are initially adsorbed onto the CS surface, they block the active sites that stop corrosion. The inhibition of these processes becomes increasingly apparent as the inhibitor concentration increases, increasing the inhibition efficiency. When the inhibitors are initially adsorbed onto the CS surface, they block the active sites that stop corrosion. Steer clear. The inhibitor molecule thus operates as a mixed type inhibitor.[52] Using the E_{corr}, the inhibitor can also be categorized as anodic, cathodic, or hybrid type. The displacement in corrosion potential ($\Delta E_{corr} = 13$ mV) in the presence of the inhibitor was less than 85 mV compared with the blank solution, indicating that the inhibitor acts as a mixed-type inhibitor affecting both the anodic metal dissolution and the cathodic hydrogen evolution reactions.[53] The shift in the E_{corr} value is less than 85 mV (13 mV) if the corrosion inhibitor is a mixed variety. The PF-1 and PF-2 compounds that are being studied in this work appear to be mixed-type inhibitors, mostly exhibiting anodic behavior. The E_{corr} result indicates an increase in the positive zone with a maximum displacement of no more than 85 mV (13 mV). Inhibitors significantly reduce the corrosion current density values when compared to those without inhibitors, as Table 6 demonstrates. Furthermore, PF-1's corrosion current density (i_{corr}) value is at its lowest level, indicating that the metal's surface has built a protective inhibitor shell.

3.3.2 Electrochemical impedance spectroscopy (EIS). The Nyquist and Bode bends of "CS in 0.5 M H_2SO_4 solutions holding altered concentration of porphyrin PF-1 & PF-2 at 25 °C" are shown in Fig. 8 and 9. "Nyquist plots, which correspond to one-time constant phase elements, show a semicircle capacitive loop that represents the entire frequency range of the blank and inhibitor solutions under investigation. When PF-1 and PF-2 inhibitors are present, the semicircle is bigger than in the blank system. The diameters of the semicircles grew as the

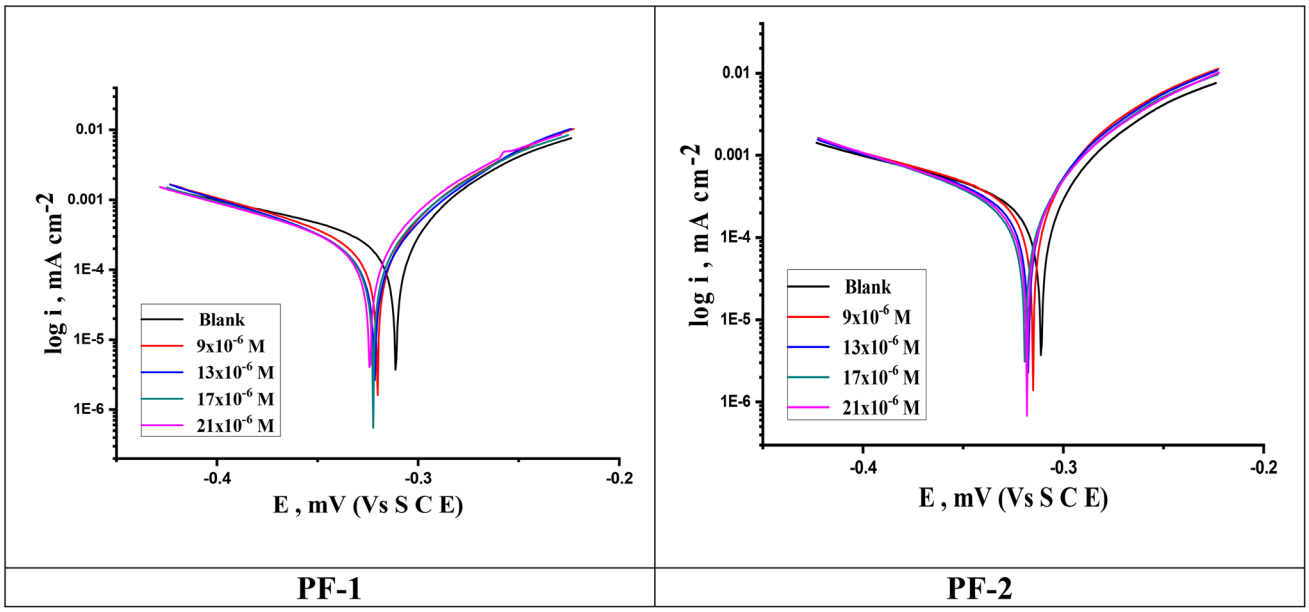

Fig. 7 PDP bends for the dissolution of CS in 0.5 M H_2SO_4 in the absence and presence of altered concentrations of porphyrin compounds.

Table 6 The polarization parameters for CS in 0.5 M H_2SO_4 in the absence and presence of various concentrations of inhibitors

Inh.	Conc., M	$-E_{corr.}$, mV *vs.* SCE	$i_{corr.}$ μA cm^{-2}	$-\beta_c$, mV dec^{-1}	β_a, mV dec^{-1}	$k_{corr.}$ mg cm^{-2} min^{-1}	θ	% η
PF-1	Blank	311 ± 10	998 ± 7	41 ± 2	156 ± 1	0.5232 ± 0.001	—	—
	9×10^{-6}	320 ± 1	197 ± 9	44 ± 3	133 ± 2	0.4458 ± 0.003	0.803	80.3
	13×10^{-6}	321 ± 3	142 ± 8	46 ± 1	136 ± 2	0.3708 ± 0.004	0.858	85.8
	17×10^{-6}	322 ± 4	109 ± 7	45 ± 1	138 ± 3	0.3391 ± 0.005	0.891	89.1
	21×10^{-6}	324 ± 5	65 ± 4	45 ± 3	133 ± 3	0.321 ± 0.003	0.935	93.5
PF-2	9×10^{-6}	315 ± 6	230 ± 6	38 ± 2	146 ± 3	0.5525 ± 0.003	0.770	77.0
	13×10^{-6}	317 ± 4	188 ± 5	41 ± 2	149 ± 2	0.5271 ± 0.002	0.812	81.2
	17×10^{-6}	319 ± 5	125 ± 4	42 ± 1	132 ± 1	0.4940 ± 0.003	0.875	87.5
	21×10^{-6}	318 ± 6	98 ± 6	43 ± 3	138 ± 1	0.4750 ± 0.004	0.902	90.2

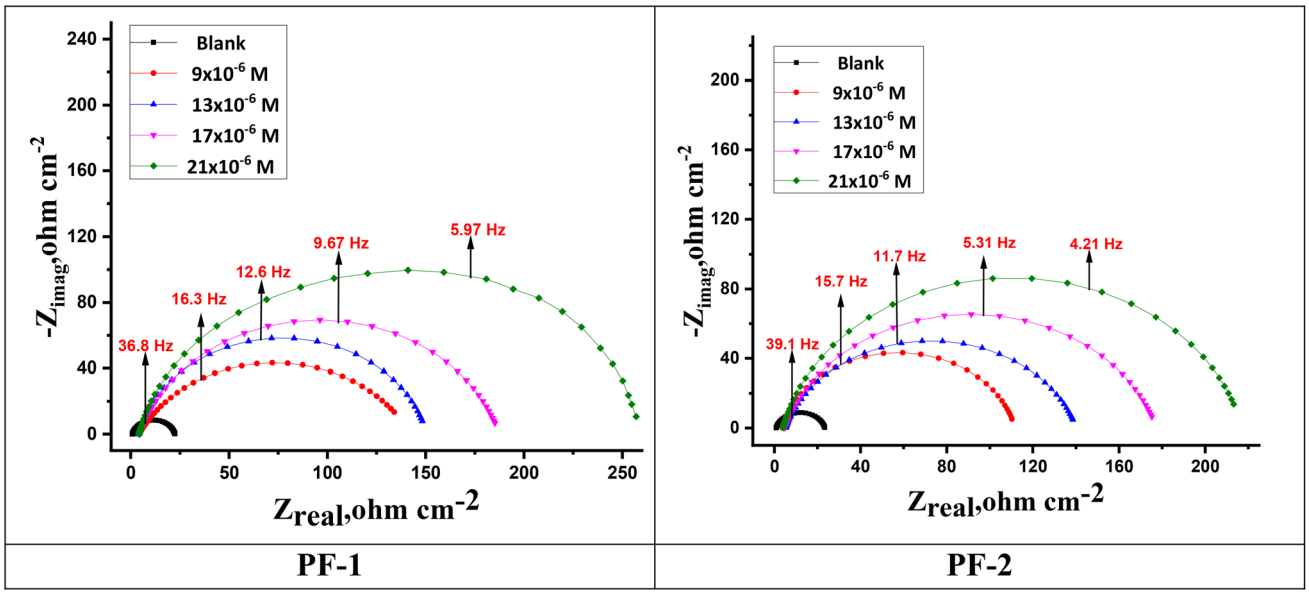

Fig. 8 Nyquist bends for C–S corrosion in the 0.5 M H_2SO_4 solutions in the absence and attendance of various concentrations of porphyrin (PF-1 & PF-2) at 25 °C.

concentration of the corrosion inhibitor increased, as seen in Fig. 8. Because of the roughness and inhomogeneity of the electrode surface, which may be related to the frequency dispersion effect, these Nyquist bends non-0.5 M H_2SO_4 are not perfect semicircles. Fig. 10 shows an equivalent circuit with a constant phase element (CPE), solution resistance (R_s), and charge transfer resistance (R_{ct}). This circuit's three parts fit the exploratory data well. This outcome showed that in the inhibited system, the CS sample was corrosion-protected.[54,55] The examination of the Nyquist bends indicates that the corrosion process was mostly charged-transfer regulated since the bends can be roughly characterized by a single capacitive semicircle."[45] The impedance of constant phase element (CPE) is described by the eqn (16):

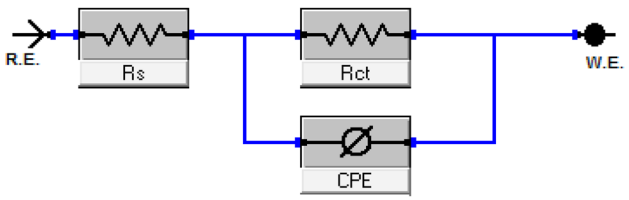

Fig. 10 Equivalent circuit used to fit experimental EIS data.

$$Z_{CPE} = Y_0^{-1}(j\omega)^{-n} \quad (16)$$

where, "Y_0 is the magnitude of the CPE and n is the deviation parameter of the CPE: $-1 \leq n \leq 1$. The values of the interfacial

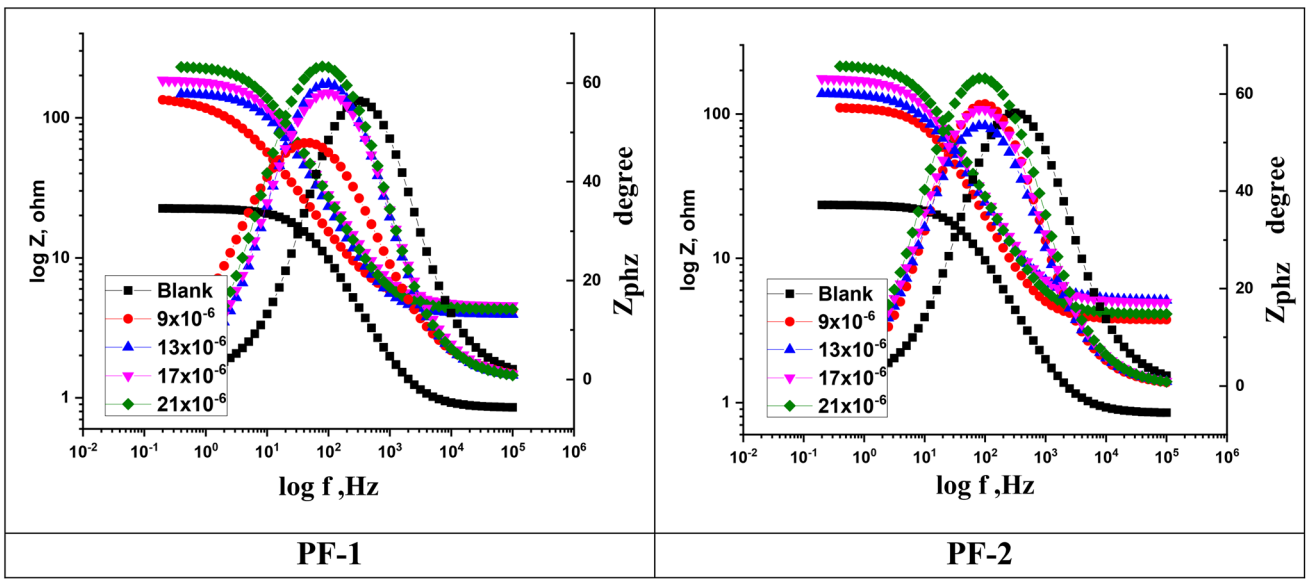

Fig. 9 Bode diagrams for the dissolution of CS in 0.5 M H_2SO_4 in the with and lack of altered dosage of porphyrin (PF-1 & PF-2) at 25 °C.

Table 7 The electrochemical impedance parameters for CS in 1 M HCl in the presence and absence of various concentration of inhibitors

Inh.	Conc., M	C_{dl} μF cm^{-2}	R_{ct} Ω cm^2	θ	% η	Goodness of fit (χ^2)
PF-1	Blank	362 ± 1.2	20 ± 1.2	—	—	19.24×10^{-3}
	9×10^{-6}	216 ± 1.3	138 ± 1.7	0.855	85.5	18.33×10^{-3}
	13×10^{-6}	149 ± 1.3	146 ± 1.5	0.863	86.3	20.25×10^{-3}
	17×10^{-6}	115 ± 1.2	182 ± 1.6	0.890	89.0	19.25×10^{-3}
	21×10^{-6}	91 ± 1.4	251 ± 1.5	0.920	92.0	16.27×10^{-3}
PF-2	9×10^{-6}	242 ± 1.2	108 ± 1.3	0.815	81.5	17.24×10^{-3}
	13×10^{-6}	200 ± 1.3	135 ± 1.6	0.852	85.2	19.25×10^{-3}
	17×10^{-6}	189 ± 1.5	172 ± 1.3	0.884	88.4	19.99×10^{-3}
	21×10^{-6}	109 ± 1.4	213 ± 1.5	0.906	90.6	18.77×10^{-3}

capacitance C_{dl} can be calculated from CPE parameter values Y_0 and n using eqn (17)":[46]

$$C_{dl} = Y_0(\omega_{max})^{n-1} \quad (17)$$

The values of the derived parameters of EIS fitting as C_{dl}, R_{ct} and IE % are listed in Table 7. When an inhibitor molecule is present, the Bode phase charts in Fig. 8 display a single time constant. "As the inhibitor concentration rises, only one phase angle peak moves more negatively. A greater negative phase angle value denotes a larger inhibitory effect because inhibitor chemicals are adsorbed at high quantities (Fig. 8). These findings demonstrate that the corrosion rate is decreased by the presence of inhibitors and further decreases as the inhibitor concentration increases. Table 7 shows that when inhibitors are added to a solution, the value of R_{ct} rises relative to the blank solution. The R_{ct} value rises when a protective barrier develops at the metal surface interface. The decline in C_{dl} values, which might be caused by an increase in the thickness of the electric double layer or a decrease in the local dielectric constant, indicates that the PF-1 and PF-2 compounds operate by adsorption at the metallic surface contact. Furthermore, it was demonstrated that the effectiveness of corrosion inhibition increased as inhibitor concentrations increased, peaking at 92% (PF-1) and 90.6% (PF-2) at an ideal concentration of 21×10^{-6} M". The impedance spectroscopy research is in line with the weight loss and potentiodynamic polarization studies.

3.4 Surface analysis

3.4.1 SEM tests. To determine if the surface morphology was changed by adding 21×10^{-6} M of porphyrin derivatives

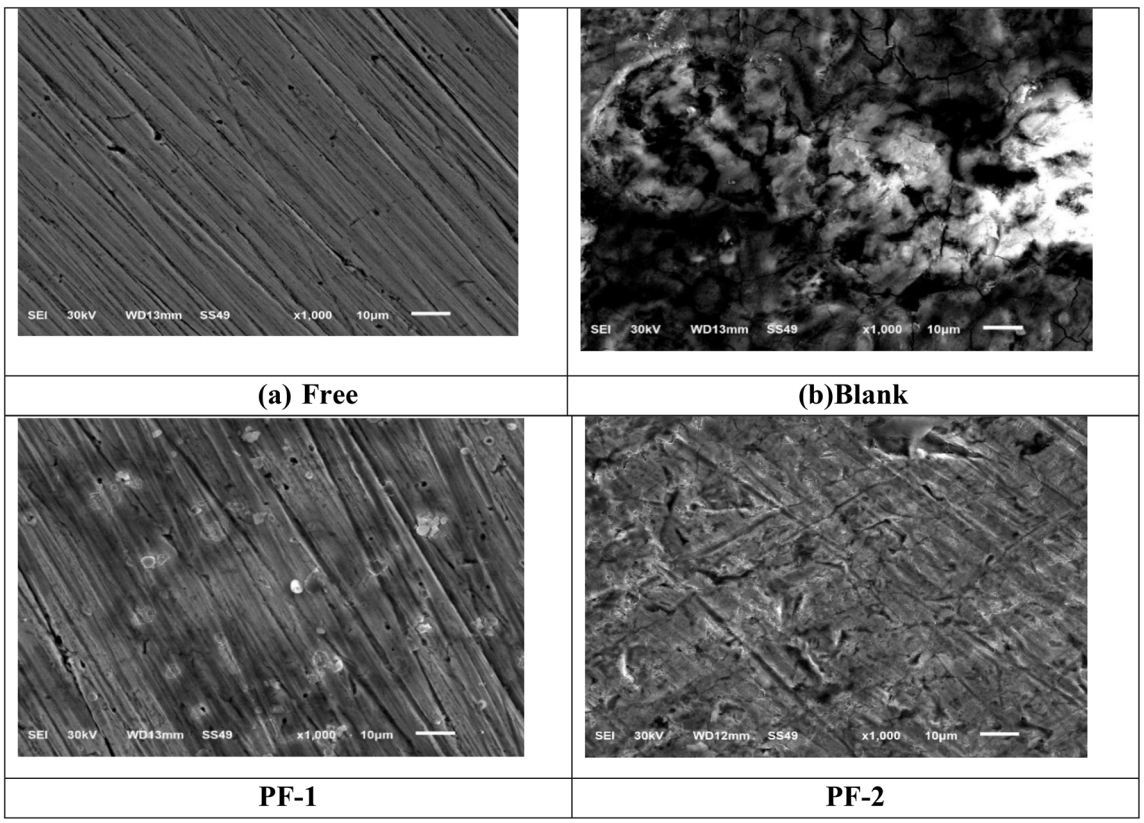

Fig. 11 SEM pictures for (a) free, (b) After of 24 h sinking in 0.5 molar H_2SO_4, (c and d) in the existence of porphyrin derivatives (1 & 2).

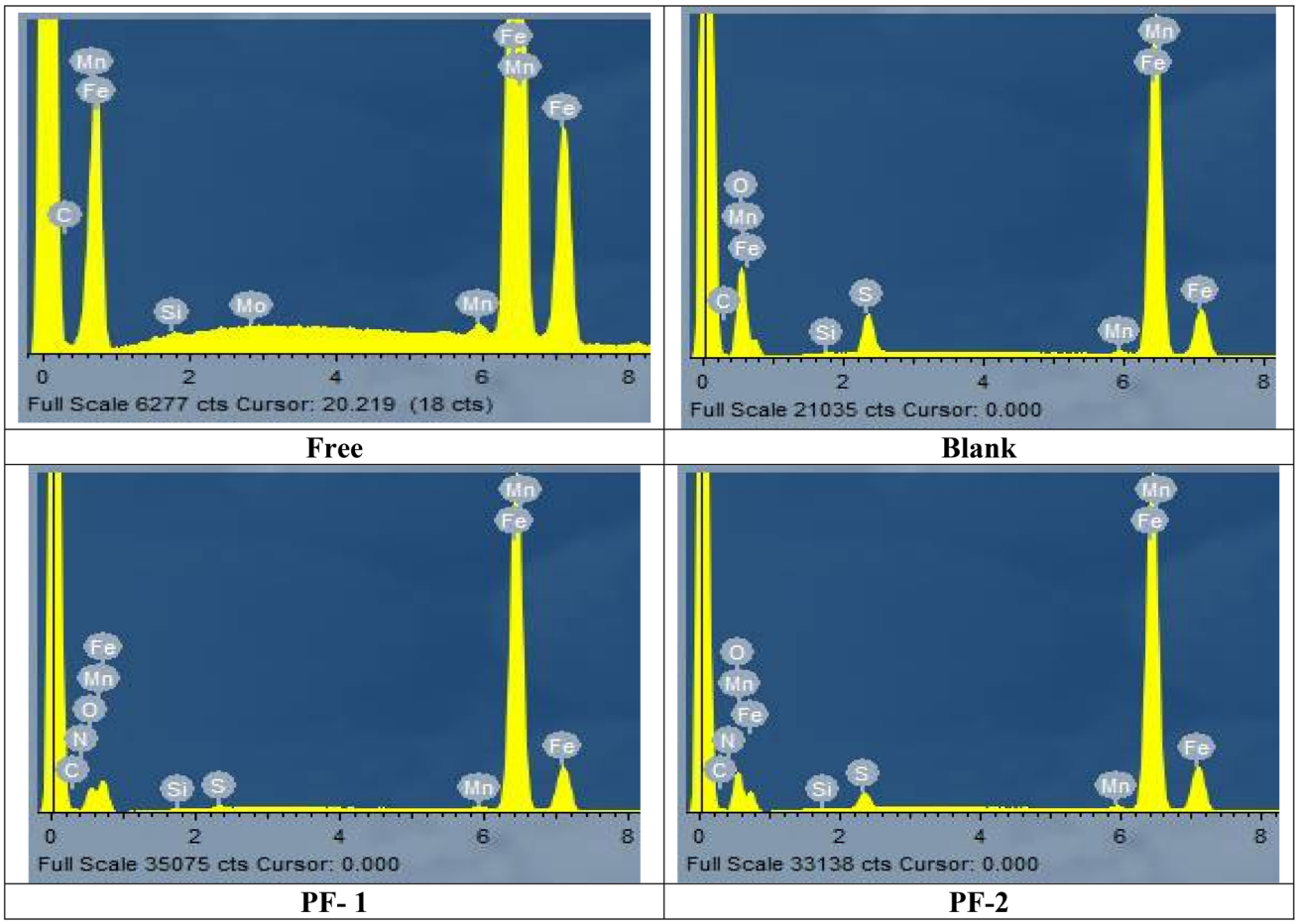

Fig. 12 EDX analysis of CS was conducted after 24 h immersion in the absence and in the presence of 21 × 10^{-6} M of the investigated inhibitors (1 and 2).

Table 8 Elemental surface composition (wt%) of CS after 24 h immersion in 0.5 M H_2SO_4 solution,in the absence and at the optimum concentration of the investigated inhibitors

(Weight %)	Fe	Mn	C	O	N	S
Pure	98.58	1.21	0.21	—	—	—
Blank	86.66	0.97	1.12	8.51	—	3.74
PF-1	75.3	0.89	0.19	11.1	12.4	0.12
PF-2	77.12	0.78	0.17	10.59	11.1	0.24

and without it, the CS surface was analyzed using "SEM as shown in Fig. 11". The CS surface was examined using SEM after a 24 hours immersion in H_2SO_4 (0.5 M), and the CS was tested both with and without the use of 21 × 10^{-6} M from compounds PF-1 & PF-2. The surface of the CS was severely damaged by corrosion in H_2SO_4 (0.5 M) in the absence of any inhibitor. After using the inhibitors, the CS surface was examined and discovered to be smooth. The presence of porphyrin derivatives in the solution lowers the rate of corrosion, improving surface shape and reducing surface roughness because they offer a robust protective layer between the CS and the corrosive medium PF-1.

3.4.2 EDX tests. As seen in Fig. 12, the EDX spectrum of CS in the uninhibited solution showed distinctive signals that corresponded to the composition of the steel and the corrosion products (O, N, and S). The elemental analysis supported the SEM findings, which showed a decrease in the O and N signal and an increase in the Fe and C peaks. The adsorption of inhibitor PF-1 and PF-2 molecules on the CS surface was confirmed by the notable development of N peaks upon the addition of inhibitors 1 and 2 (Table 8). These results demonstrate the strong surface-blocking power of inhibitors 1 and 2 in protected CS corrosion and validate the protective film generation.[56]

3.4.3 AFM analysis. The surface morphology of CS was examined using AFM measurements after immersion in 0.5 M H_2SO_4 solution, both in the absence and presence of 21 × 10^{-6} M PF-1 and PF-2 for 24 hours and was evaluated in terms of surface roughness (Fig. 13). The average roughness value (S_a) of the surface profile plays a crucial role in identifying and reporting the effectiveness of the tested inhibitor.[57] Surface roughness, among other factors, contributes to explaining the nature of the layer adsorbed on the CS surface. Fig. 13a illustrates the polished metal surface (S_a = nm), while Fig. 13b shows the metal surface after exposure to sulphuric acid,

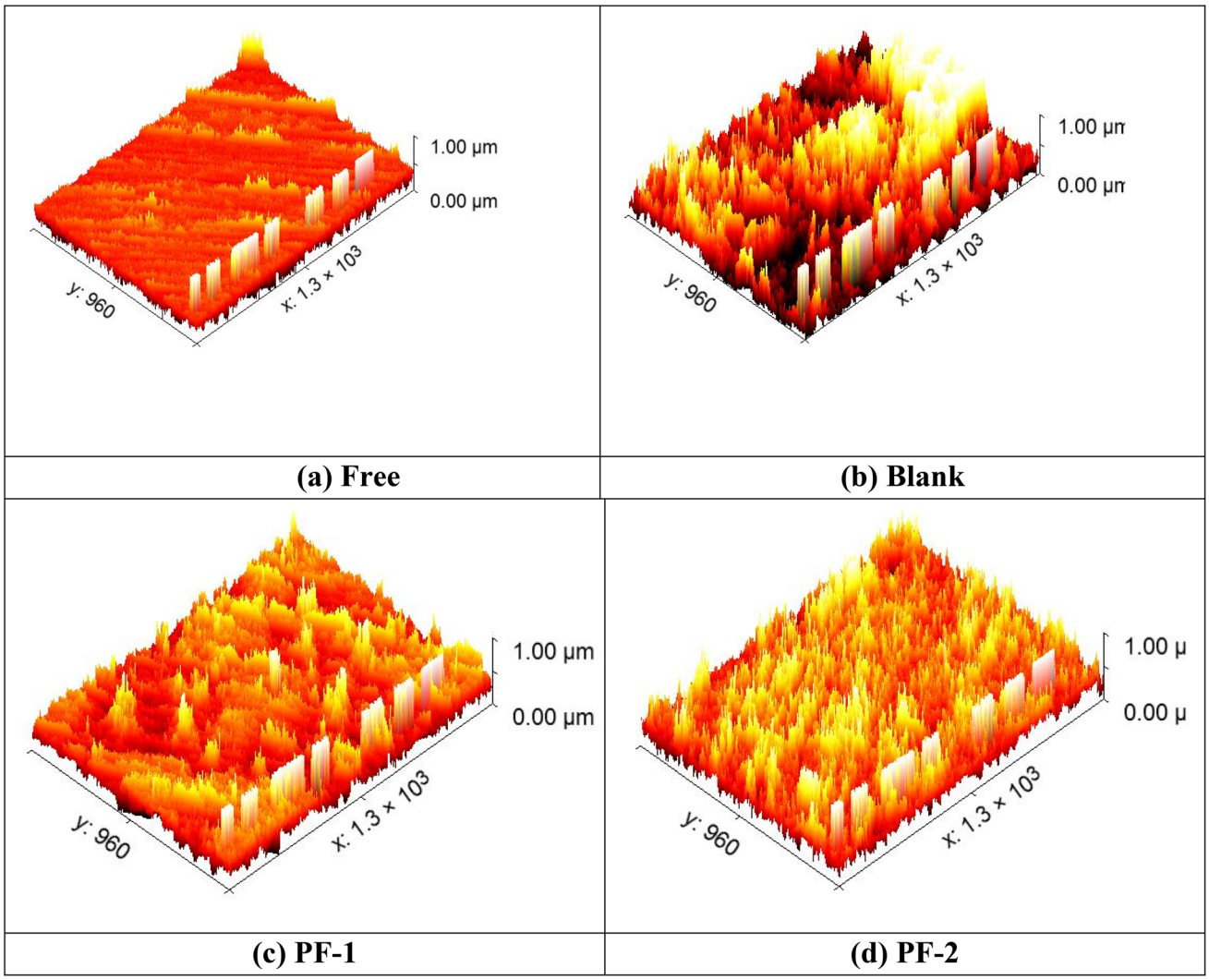

Fig. 13 AFM images of C-steel in H_2SO_4: (a) before immersion in H_2SO_4, (b) after immersion in H_2SO_4, (c) after immersion in H_2SO_4 + 21 × 10^{-6} M PF-1 and (d) after immersion in H_2SO_4 + 21 × 10^{-6} M PF-2.

exhibiting severe damage and a high roughness value (S_a = 820 nm). In contrast, Fig. 13c and d display the CS surface in the presence of 21 × 10^{-6} M PF-1 and PF-2, respectively, where the surface is less susceptible to corrosion and shows significantly lower roughness values of 147 and 190 nm, respectively.

3.5 Quantum chemical parameters

Fig. 14 shows the Frontier molecular orbitals of the inhibitors system. The energy band gap ΔE ($\Delta E = E_{HOMO} - E_{LUMO}$), which represents the lower energy band gap value, shows that organic molecules are very reactive and have good corrosion behavior on the CS surface. Numerous parameters have been obtained from the computations. The energies of the highest (E_{HOMO}) occupied and lowest (E_{LUMO}) empty molecular orbitals were computed. Ionization potential ($I_p = -E_{HOMO}$), molecular dipole moment (μ), electron affinity ($E_A = -E_{LUMO}$), global hardness (η), electronegativity (χ) that are used to calculate the electrons transfer from the inhibitor molecule to the metallic atom ΔN, electrophilicity index (ω), softness (σ), and back-donation ($\Delta E_{back\text{-}donation}$) were all calculated using Koopmans's theorem[58] from the following balance:

$$\mu = -\chi = -\frac{I_p + E_A}{2} \quad (18)$$

$$\chi = \frac{I_p + E_A}{2} \quad (19)$$

$$\eta = \frac{I_p - E_A}{2} \quad (20)$$

$$\sigma = \frac{1}{\eta} \quad (21)$$

$$\omega = \frac{\mu^2}{2\eta} \quad (22)$$

$$\Delta E_{back\text{-}donation} = -\frac{\eta}{4} \quad (23)$$

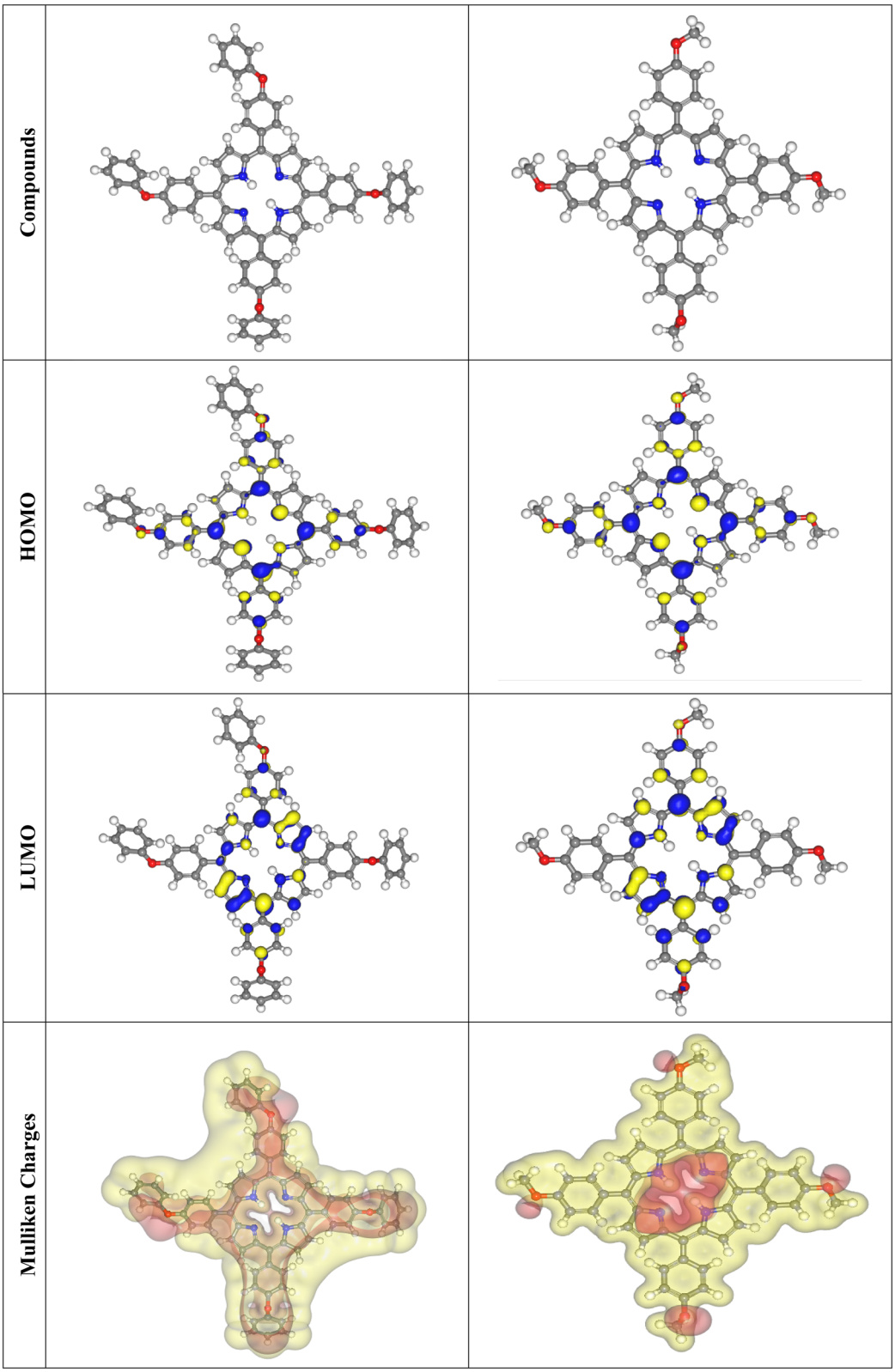

Fig. 14 HOMO and LOMO planned for the tested organic derivatives at DMol3.

Table 9 QM data for the organic inhibitors under study

Compound	PF-1	PF-2
E_{HOMO}, eV	−4.435	−4.545
E_{LUMO}, eV	−3.612	−3.677
ΔE, eV	0.82	0.87
I_P, eV	4.435	4.545
E_A, eV	3.612	3.677
η, eV	0.41	0.43
σ, eV	2.43	2.30
ω	19.67	19.47
ΔN	3.62	3.33
($\Delta E_{back\text{-}donation}$)	−0.10	−0.11
Dipole moment (debye)	6.95	3.05

Because of this, inhibitor (PF-1) has a greater capacity to shield the CS surface than inhibitor (PF-2). Compound (PF-1) has the largest ΔN (FET) value, indicating a higher affinity to share electrons with the CS surface than inhibitors (PF-2), as shown in Table 9. The polarity of the substances under investigation was determined by the covalent bond (μ). High values are known to increase the tested chemicals' propensity to adsorb on metal surfaces.

The gross charge of atom k is represented by q_k, while N is the total number of electrons in the molecule. The neutral molecule's LUMO was altered by adding and subtracting the electrons $N + 1$ and $N - 1$, which stand for the anion and cation, respectively. Tables S1 and S2 provide an overview of the Fukui index analysis. Nitrogen and oxygen are shared by all the organic inhibitors that are being studied. For nucleophilic assault, the nitrogen support value is therefore more suitable. Of the two inhibitors, PF-1's nitrogen has the highest value of f_k^+ (0.0.011), indicating that it serves as a superior nucleophilic site. Nitrogen and oxygen are good electrophilic sites in PF-2, with values of $f_k^- = 0.027$ and 0.012, respectively. Research on Fukui activities indicates that PF-1 is a more potent inhibitor than PF-2.

3.6 MC simulations

3.6.1 Monte Carlo (MC) simulation. To learn more about the interactions between the molecules under investigation and the metal surface in an acidic and vacuum environment, "Monte Carlo simulation was used. Views from the top and sides of the more robust configuration for the adsorption of porphyrin derivatives (PF-1 & PF-2) on the surface of cleaved Fe(110) (Fig. 15). To identify the optimal adsorption locations, MC stimulation using an adsorption lector module detects the

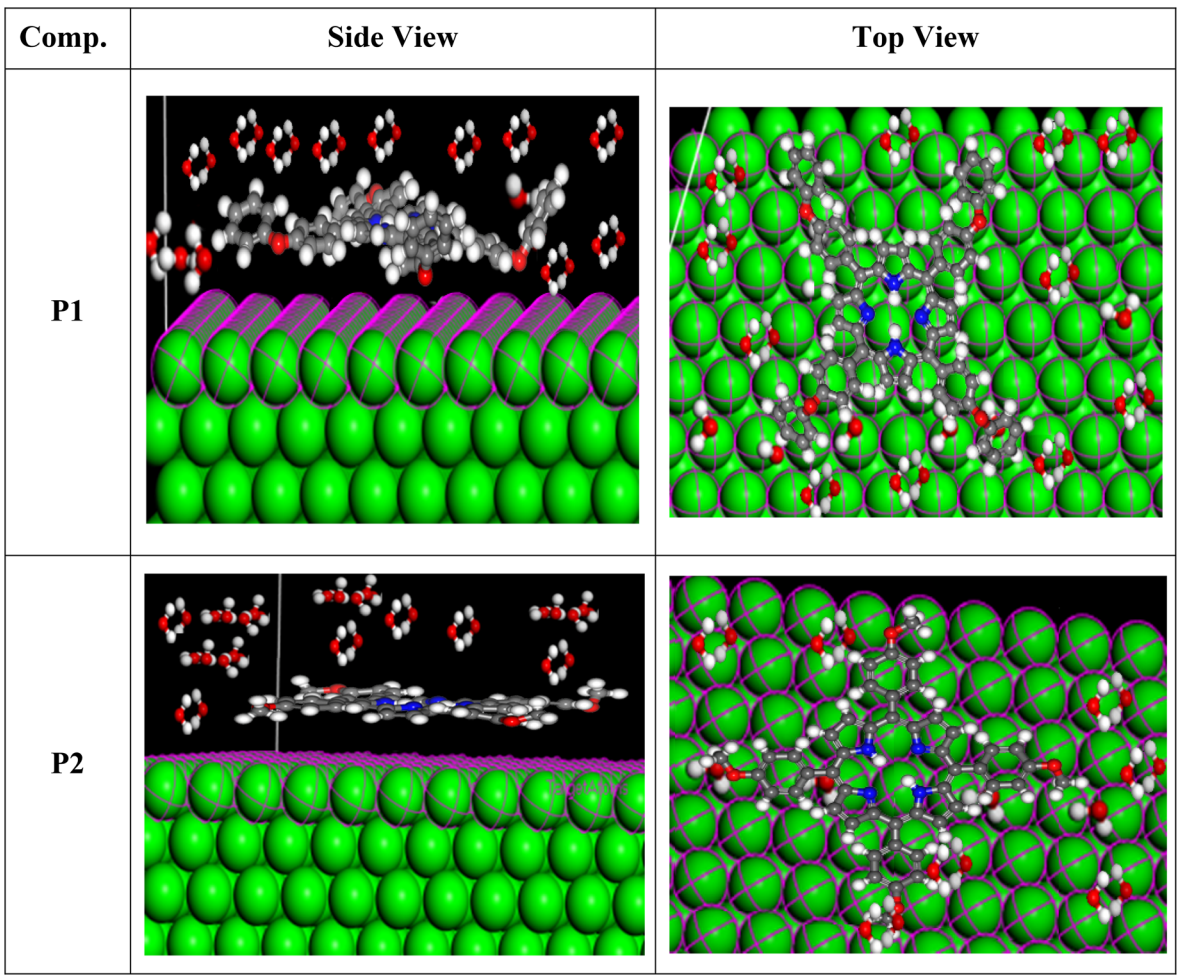

Fig. 15 Adsorption configurations of the porphyrins molecules on the iron surface.

Table 10 Monte Carlo simulation parameters of adsorption of porphyrins molecules on Fe(110) surface

Structures	Adsorption energy	Rigid adsorption energy	Deformation energy	Compound dE_{ad}/dNi	H_2O dE_{ad}/dNi
Fe(110)/PF1/H_2O	−5340.995	−5534.425	193.43	−310.37	−12.64
Fe(110)/PF2/H_2O	−4904.443	−5091.363	186.92	−287.55	−11.18

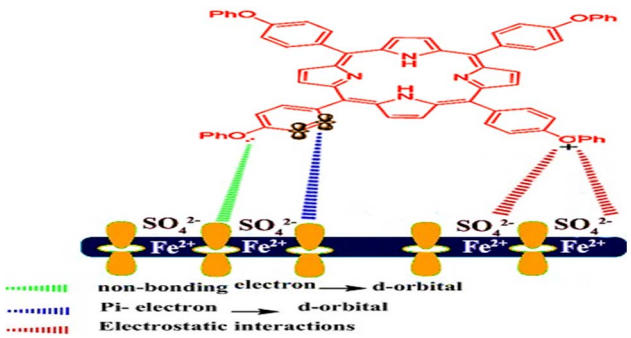

Fig. 16 Mechanism of the corrosion inhibition.

interaction between inhibitors and the surface area of the Fe(110) crystal.[59] Low-energy configurations of the Fe(110)-inhibitor system in aqueous solution are examined in this work. The simulation was carried out in an aquatic environment with water molecules to replicate corrosion in a real-life setting. The adsorption configuration, which is almost parallel in position due to the inhibitor molecule's relaxation on Fe(110), is shown in Table 10. Table 10 displays the descriptors calculated from MC stimulation. For porphyrins (PF-1, PF-2), the calculated adsorption energies are −5340.995 and −4904.443 kcal mol^{-1}, respectively". The results demonstrate that both inhibitors are effective adsorptive inhibitors, with porphyrin (PF-1) being the superior inhibitor based on the experimental findings. Porphyrin (PF-1) has the most negative rigid adsorption energies at −5534.425 (PF-1) and −5091.363 (PF-2) kcal mol^{-1}, while porphyrin (PF-1) has the highest deformation energies at 193.43 (PF-1) and 186.92 (PF-2) kcal mol^{-1}, respectively, confirming that porphyrin (PF-1) has a stronger inhibitory effect than porphyrin (PF-2). When comparing dE_{ad}/dNi for inhibitors (−310.37, −287.55) kcal mol^{-1} and dE_{ad}/dNi for water (−12.64, −11.18) kcal mol^{-1}, it is discovered that the values for water are significantly lower than those for inhibitors, indicating the replacement of water molecules by inhibitor molecules. This is because dE_{ad}/dNi provides information about the metal adsorbents as if they are adsorbed or ignored. Theoretical modeling makes it clear that porphyrins are potent inhibitors of carbon steel, and experimental and spectral analysis supports this. Based on IE%, the prepared inhibitors are ranked PF-1 > PF-2.

4 Mechanism of inhibition

Organic inhibitors mainly stop CS corrosion by transferring H_2O molecules to the CS's surface and sticking to them, creating a thick barrier layer.[60] "The protective potential patterns of the two compounds are found to be dependent on how the substituent groups PhO- and OCH_3 affect the molecules' ability to donate or take electrons. PF-1 > PF-2 is the order of increasing % IE of inhibitors from all applicable tests. The best inhibitor is PF-1 since it has a large molecular size and a strong electron-donating compound. Because inhibitor (PF-2) contains OCH_3, and less molecular size, the protection efficiency is decreased in it than PF-2. "As shown in Fig. 16, there are two different kinds of adsorption: chemical and physical. While the chemisorption process entails exchanging electrons or transferring them from the molecules to the iron's d-orbital to create a coordination bond, the physisorption process requires the presence of charged metal surfaces and charged molecules. Molecular adsorption and the potential electrical density of active centers, such as N and S. In an acidic solution, the CS sample's surface has a positive charge". The negatively charged metal surface created by the adsorbed SO_4^{2-} ions on the CS sample attracts the protonated molecules (cationic) electrostatically".

5 Conclusions

The following conclusions can be listed based on the earlier findings:

The inhibitory process increased with increasing concentrations of certain substances and decreased with increasing temperature, according to values derived from MR measurements. At a concentration of 21×10^{-6} M in a 1 M HCl solution, PF-1 demonstrated a maximum inhibitory performance of 95.9%. The chosen inhibitors primarily exhibited physical adsorption on the CS surface, adhering to the Langmuir adsorption isotherm. Measurements of PDP demonstrate that these substances function as mixed-type inhibitors. When varying amounts of the chosen chemicals were introduced, the EIS findings demonstrated that the double layer capacitance values (C_{dl}) decreased and the charge transfer resistance (R_{ct}) increased. This results from the inhibitor molecules of the chosen chemicals adhering to the metal surface. Quantitative chemistry metrics including energy gap (ΔE), E_{LUMO}, and chemical softness are compatible with several experimental research, and the theoretical studies' calculations show a relationship between the investigated compounds' inhibitory efficiency and their structural parameters. The order of inhibitor molecules for the CS electrode in an acidic solution is as follows, based on both theoretical and experimental research: PF-1 > PF-2. Surface area, the quantity of heteroatoms, and functional groups are the causes of this behavior. The fact that the outcomes from every technique were very consistent with

one another was intriguing. In summary, every molecule examined in this work has demonstrated promise as a corrosion inhibitor for CS corrosion in acidic settings. However, the study is confined to controlled laboratory conditions and does not consider long-term stability or the effects of industrial variables such as temperature and flow. Furthermore, the structure–activity relationships were not fully established. Future work should concentrate on the design of substituted porphyrins, the evaluation of their performance under realistic conditions, and the application of advanced surface characterization techniques and theoretical approaches to achieve a deeper understanding of adsorption mechanisms and enhance inhibitor efficiency.

Conflicts of interest

There are no conflicts to declare.

Data availability

The data that support the findings of this study are available from the corresponding author, [A. S. Fouda], upon reasonable request.

Supplementary information (SI) is available. See DOI: https://doi.org/10.1039/d6ra00078a.

References

1 A. S. Fouda, H. E. Megahed, N. Fouad and N. M. Elbahrawi, Corrosion inhibition of carbon steel in 1M hydrochloric acid solution by aqueous extract of *Thevetia peruviana*, *J. Bio Tribo Corros.*, 2016, **2**(3), 1–16.
2 Y. G. Avdeev, T. A. Nenasheva, A. Y. Luchkin, A. I. Marshakov and Y. I. Kuznetsov, Thin1,2,4-triazole films for the inhibition of carbon steelcorrosion in sulfuric acid solution, *Coatings*, 2023, **13**(7), 1217–1221.
3 D. Dwivedi, K. Lepkova and T. Becker, Carbon steel corrosion: A review of key surface properties and characterization methods, *RSC Adv.*, 2017, **7**(8), 4580–4610.
4 Y. Fukaya and Y. Watanabe, Characterization and prediction of carbon steel corrosion in diluted seawater containing pentaborate, *J. Nucl. Mater.*, 2018, **498**, 159–168.
5 K. Zhang, B. Xu, W. Yang, X. Yin, Y. Liu and Y. Chen, Halogen-substituted imidazoline derivatives as corrosion inhibitors for mild steel in hydrochloric acid solution, *Corros. Sci.*, 2015, **90**, 284–295.
6 L. T. Popoola, A. S. Grema, G. K. Latinwo, B. Gutti and A. S. Balogun, Corrosion problems during oil and gas production and its mitigation, *Int. J. Ind. Chem. Biotechnol.*, 2013, **4**(1), 35–50.
7 A. Singh, K. R. Ansari, A. Kumar, W. Liu, C. Songsong and Y. Lin, Investigation of Corrosion Inhibitors Adsorption on Metals Using Density Functional Theory and Molecular Dynamics Simulation, *J. Alloys Compd.*, 2017, **712**, 121–140.
8 I. B. Onyeachu, M. M. Solomon, S. A. I. B. Obot and A. A. Sorour, Corrosion inhibition effect of a benzimidazole derivative on heat exchanger tubing materials during acid cleaning of multistage flash desalination plants, *Desalination*, 2020, **479**, 114283.
9 J.-H. Chou, M. E. Kosal, H. S. Nalwa, N. A. Rakow and K. S. Suslick, Applications of Porphyrins and Metalloporphyrins to Materials Chemistry, *Porphyrin Hand Book*, 2000, vol. 6, pp. 43–131.
10 K. J. Barnham, C. L. Masters and A. I. Bush, Neurodegenerative diseases and oxidative stress, *Nat. Rev. Drug Discov.*, 2004, **3**, 205–214.
11 K. S. Lokesh, M. de Keersmaecker and A. Adriaens, Self-assembled films of porphyrins with amine groups at different positions: Influence of their orientation on the corrosion inhibition and the electrocatalytic activity, *Molecules*, 2012, **17**, 7824–7842.
12 K. Jomova, D. Vondrakova, M. Lawson and M. Valko, Metals, oxidative stress and neurodegenerative disorders, *Mol. Cell. Biochem.*, 2010, **345**, 91–104.
13 K. M. Kadish, K. M. Smith and R. Guilard, *The Porphyrin Handbook*, New York, NY, US. Academic press, 2000, vol. 14, pp. 55–63.
14 H. M. Yang, Role of Organic and Eco-Friendly Inhibitors on the Corrosion Mitigation of Steel in Acidic Environments—A State-of-Art Review, *Molecules*, 2021, **26**, 3473.
15 W. Su, T. M. Cooper and M. C. Brant, Large Optical-Limiting Response in Some Solution-Processable Polyplatinaynes, *Chem. Mater.*, 2005, **17**(20), 5209–5217.
16 H. Ali and J. E. Lier, Metal complexes as photo-and radiosensitizers, *Chem. Rev.*, 1999, **99**, 2379.
17 T. H. El-Mokadem, A. I. Hashem, N. E. A. A. El-Sattar, E. A. Dawood and N. S. Abdelshafi, Green synthesis, electrochemical, DFT studies and MD simulation of novel synthesized thiourea derivatives on carbon steel corrosion inhibition in 1.0 M H2SO4, *J. Mol. Struct.*, 2023, **1274**, 134567.
18 T. Koopmans, The classification of wave functions and eigen-values to the single electrons of an atom, *Physica*, 1934, **1**, 104–113.
19 A. S. Fouda, A. El-Mekabaty, I. E. Shaaban and A. El-Hossiany, Synthesis and Biological Evaluation of Novel Thiophene Derivatives as Green Inhibitors for Al Corrosion in Acidic Media, *Protect. Met. Phys. Chem. Surface*, 2021, **57**(5), 1060–1075.
20 F. R. Longo, Corrosion and anti-corrosives, in *PORPHYRINS as Corrosion Inhibitors*, Naval Air Development Center Warminster, PA, USA, 1984.
21 M. Biesaga, K. Pyrzyńska and M. Trojanowicz, Porphyrins in analytical chemistry. A review, *Talanta*, 2000, **51**, 209–224.
22 J. Xiao and M. E. Meyerhoff, Retention behavior of amino acids and peptides on protoporphyrinsilica stationary phases with varying metal ion centers, *Anal. Chem.*, 1996, **68**, 2818–2825.
23 Z. Shi and C. Fu, Porphyrins as ligands for trace metal analysis by high-performance liquid chromatography, *Talanta*, 1997, **44**, 593–604.
24 S. Hettiarachichi, Y. W. Chan, R. B. Wilson, Jr and V. S. Agarwala, Macrocyclic corrosion inhibitors for steel in acid chloride environments, *Corrosion*, 1989, **45**, 30–34.

25 S. L. A. Maranhao, I. C. Guedes, F. J. Anaissi, H. E. Toma and I. V. Aoki, Electrochemical and corrosion studies of poly(nickel-tetraaminophthalocyanine) on carbon steel, *Electrochim. Acta*, 2006, **52**, 519–526.

26 M. T. Jaafar, L. M. Ahmed and R. T. Haiwal, Novel Porphyrin Derivatives and Investigate their Application in Sensitized Solar Cells, *Iraqi j. chem. pet. eng.*, 2023, **42**(2), 113–122.

27 A. S. Fouda, H. M. Abdel-Wahed, M. F. Atia and A. El-Hossiany, Novel porphyrin derivatives as corrosion inhibitors for stainless steel 304 in acidic environment: synthesis, electrochemical and quantum calculation studies, *Sci. Rep.*, 2023, **13**, 17593.

28 M. Thamer Jaafar, L. Majeed Ahmed and R. T. Haiwal, Synthesis, Characterization, and Electrochemical Study of Novel Porphyrin Derivatives as Corrosion Inhibitors for Carbon Steel in HCl Solutions, *Indones. J. Chem.*, 2024, **24**(2), 379–389.

29 M. Belhadi, O. Roby, M. Baadi, M. Chafi, O. Dagdag, H. Kim, A. Berisha, R. Haldhar, S.-C. Kim and S. Tighadouini, Investigation of the adsorption and inhibition mechanisms of new pyrazole derivatives on carbon steel corrosion in 1 M HCl acid solution: experimental analysis and quantum chemistry, *J. Mater. Sci.*, 2025, **60**, 14749–14772.

30 Q. A. Yousif, Z. Fadel, A. M. Abuelela, E. H. Alosaimi, S. Melhi and M. A. Bedair, Insight into the corrosion mitigation performance of three novel benzimidazole derivatives of amino acids for carbon steel (X56) in 1 M HCl solution, *RSC Adv.*, 2023, **13**, 13094.

31 A. S. Fouda, H. M. Abdel-Wahed, M. F. Atia and A. El-Hossiany, Novel porphyrin derivatives as corrosion inhibitors for stainless steel 304 in acidic environment: synthesis, electrochemical and quantum calculation studies, *Sci. Rep.*, 2023, **13**, 17593.

32 M. A. Quraishi and J. Rawat, A review on macrocyclic as corrosion inhibitors, *Corros. Rev.*, 2011, **19**(3–4), 273.

33 Y. Feng, S. Chen, W. Guo, G. Liu, H. Ma and L. Wu, Electrochemical and molecular simulation studies on the corrosion inhibition of 5,10,15,20-tetraphenylporphyrin adlayers on iron surface, *Appl. Surf. Sci.*, 2007, **253**, 8734–8874.

34 G. Fagadar-Cosma, B. O. Taranu, M. Birdeanu, M. Popescu and E. Fagadar-Cosma, Influence of 5,10,15,20-tetakis(4-pyridyl)-21H,23H-Porphyrin on the corrosion of steel in aqueous sulfuric acid, *Dig. J. Nanomater. Biostruct.*, 2014, **9**(2), 551–557.

35 I. Popa, E. Fagadar-Cosma, B.-O. Taranu, M. Birdeanu, G. Fagadar-Cosma and I. Taranu, Corrosion protection efficiency of bilayer porphyrin-polyaniline film deposited on carbon steel, *Macromol. Symp.*, 2015, **352**, 16–24.

36 A. Singh, Y. Lin, M. A. Quraishi, L. O. Olasunkanmi, O. E. Fayemi, Y. Sasikumar, B. Ramaganthan, I. Bahadur, I. B. Obot, A. S. Adekunle, M. M. Kabanda and E. E. Ebenso, Porphyrins as corrosion inhibitors for N80 steel in 3.5% NaCl solution: electrochemical, quantum chemical, QSAR and Monte Carlo simulations studies, *Molecules*, 2015, **20**, 15122–15146.

37 A. Singh, M. Talha, X. Xu, Z. Sun and Y. Lin, Heterocyclic corrosion inhibitors for J55 steel in a sweet corrosive medium, *ACS Omega*, 2017, **2**, 8177–8186.

38 A. A. Fadda, R. E. El-Mekawy and A. I. El-Shafei, Synthesis, antiviral, cytotoxicity and antitumor evaluations of A4 type of porphyrin derivatives, *J. Porphyrins Phthalocyanines*, 2015, **19**(06), 753–768.

39 Y. El Aoufir, *et al*, The effect of the alkyl chain length on corrosion inhibition performances of 1,2,4-triazolebased compounds for mild steel in 1.0 M HCl: insights from experimental and theoretical studies, *J. Mol. Liq.*, 2020, **303**, 112631.

40 S. Bashir, V. Sharma, G. Singh, H. Lagaz, R. Salghi, A. Singh and A. Kumar, electrochemical behavior and computational analysis of phenylephrine for corrosion of Al in acidic medium, *Mater. Trans.*, 2018, **A5**, 468–479.

41 H. Lgaz, *et al*, Corrosion inhibition of mild steel in hydrochloric acid by 5,5 ',5"-(nitrilotris (methylene)) tris-(8-quinolinol): experimental, theoretical and molecular dynamic studies, *Moroccan J. Chem.*, 2016, **4**(2), 592–612.

42 M. A. Deyab, R. Essehli and B. El Bali, performance evaluation of phosphite $NaCo(H_2PO_3).H_2O$ as a corrosion inhibitor for Alin engine cooling solutions, *RSC Adv.*, 2015, **5**, 48868–48874.

43 M. A. Hegazy, A. A. Nazeer and K. Shalabi, Electrochemical studies on the inhibition behavior of copper corrosion in pickling acid using quaternary ammonium salts, *J. Mol. Liq.*, 2015, **209**, 419–427.

44 A. A. Nazeer, E. Al-Hetlani, M. O. Amin, T. Quiñones-Ruiz and I. K. Lednev, A poly (butyl methacrylate)/graphene oxide/TiO2 nanocomposite coating with superior corrosion protection for AZ31, alloy in chloride solution, *Chem. Eng. J.*, 2019, **361**, 485–498.

45 E. Motsie Mashuga, O. Lukman Olasunkanmi, S. Abolanle Adekunle, S. Yesudass, M. wadham, M. Kabanda and E. E. Ebenso, Adsorption, thermodynamic and quantum chemical studies of 1-hexyl-3-methylimidazolium based ionic liquids as corrosion inhibitors for mild steel in HCl, *Materials*, 2015, **8**, 3607–3632.

46 Y. Liu, X. Guo, B. Wang, P. Gong, Y. Liu, H. Li and Y. Wu, Lentinan as an eco-friendly corrosion inhibitor for Q235 steel in acid medium: Experimental and theoretical studies, *J. Mol. Liq.*, 2022, **360**, 119513.

47 I. B. Onyeachu, I. B. Obot, A. A. Sorour and M. I. Abdul-Rashid, Green corrosion inhibitor for oilfield application I: Electrochemical assessment of 2-(2-pyridyl) benzimidazole for API60 steel under sweet environment in nace brine, *Corros. Sci.*, 2019, **150**, 183–193.

48 A. Sánchez-Eleuterio, C. Mendoza-Merlos, R. Corona Sánchez, A. M. Navarrete-López, A. Martínez Jiménez, E. Ramírez-Domínguez, L. L. Romero, R. O. Cruz, A. E. Vázquez and G. E. Negrón-Silva, Experimental and Theoretical Studies on Acid Corrosion Inhibition of API 5L X70 Steel with Novel 1-N-α-d-Glucopyranosyl-1 H-1, 2, 3-Triazole Xanthines, *Molecules*, 2023, **28**(1), 460.

49 T. H. El-Mokadem, A. I. Hashem, N. E. A. Abd El-Sattar, E. A. Dawood and N. S. Abdelshafi, Green synthesis,

electrochemical, DFT studies and MD simulation of novel synthesized thiourea derivatives on carbon steel corrosion inhibition in 1.0 M H2SO4, *J. Mol. Struct.*, 2023, **1274**, 134567.

50 M. A. Ali, A. A. El-Hossiany, A. M. Ouf and A. S. Fouda, Assessment of corrosion restraint effect of carbon steel immersed in hydrochloric acid by expired tilmicosin drug, *Sci. Rep.*, 2025, **15**(1), 37621.

51 C. M. Fernandes, P. C. de Oliveira, V. G. Pina, B. S. Peixoto, F. F. Massante, M. C. Veloso and E. A. Ponzio, Pyrolysis of Syagrus coronata: transforming agroindustrial waste into a new environmentally sustainable corrosion inhibitor, *Sustain. Chem. Pharm.*, 2022, **29**, 100751.

52 W. Xu, X. Lu, J. Tian, C. Huang, M. Chen, Y. Yan, L. Wang, Z. Qu and C. Wen, Microsturcture, wear resistance, and corrosion performance of Ti35Zr28Nb alloy fabricated by powder metallurgy for orthopaedic applications, *J. Mater. Sci. Technol.*, 2020, **41**, 191–198.

53 S. S. Abd El Rehim, S. M. Sayyah, M. M. El-Deeb, S. M. Kamal and R. E. Azooz, Adsorption and corrosion inhibitive properties of P (2-aminobenzothiazole) on mild steel in hydrochloric acid media, *Int. J. Ind. Chem.*, 2016, **7**, 39–52.

54 N. Z. N. Hashim, M. A. M. Kahar, K. Kassim and Z. Embong, Experimental and theoretical studies of azomethines derived from benzylamine as corrosion inhibitors of mild steel in 1 M HCl, *J. Mol. Struct.*, 2020, **1222**, 128899.

55 C. Verma, M. Ahmad Quraishi, K. Kluza, M. Makowska-Janusik, L. O. Olasunkanmi and E. E. Ebenso, Corrosion inhibition of mild steel in 1M HCl by D-glucose derivatives of dihydropyrido [2, 3-d: 6, 5-d′] dipyrimidine-2, 4, 6, 8 (1H, 3H, 5H, 7H)-tetraone, *Sci. Rep.*, 2017, **7**, 1–17.

56 M. Yadav, R. R. Sinha, S. Kumar and T. K. Sarkar, Corrosion inhibition effect of spiropyrimidinethiones on mild steel in 15% HCl solution: insight from electrochemical and quantum studies, *RSC Adv.*, 2015, **5**, 70832–70848.

57 A. S. Fouda, E. S. El-Gharakawy, H. Ramadan and A. El-Hossiany, Corrosion resistance of mild steel in HCl solutions by clinopodium acinos as green inhibitor, *Biointerface Res. Appl. Chem.*, 2021, **11**, 9786.

58 H. A. Ali, A. A. El-Hossiany, A. S. Abousalem, M. A. Ismail, A. S. Fouda and E. A. Ghaith, Synthesis of new binary trimethoxyphenylfuran pyrimidinones as proficient and sustainable corrosion inhibitors for carbon steel in acidic medium: experimental, surface morphology analysis, and theoretical studies, *BMC Chem.*, 2024, **18**(1), 182–214.

59 A. S. Fouda, A. El-Mekabaty, I. E. Shaaban and A. El-Hossiany, Synthesis and Biological Evaluation of Novel Thiophene Derivatives as Green Inhibitors for Aluminum Corrosion in Acidic Media, *Protect. Met. Phys. Chem. Surface*, 2021, **57**(5), 1060–1075.

60 A. S. Fouda, S. A. Abd El-Maksoud, A. El-Hossiany and A. Ibrahim, Corrosion protection of stainless steel 201 in acidic media using novel hydrazine derivatives as corrosion inhibitors, *Int. J. Electrochem. Sci.*, 2019, **14**, 2187–2207.